ECOLOGY

Low oxygen but dynamic marine redox conditions permitted the Cambrian Radiation

Ruaridh D. Alexander[1]*, Andrey Yu. Zhuravlev[2], Fred T. Bowyer[1,3], Laetitia Pichevin[1], Simon W. Poulton[3], Artem Kouchinsky[4], Rachel Wood[1]

Whether metazoan diversification during the Cambrian Radiation was driven by increased marine oxygenation remains highly debated. Repeated global oceanic oxygenation events have been inferred during this interval, but the degree of shallow marine oxygenation and its relationship to biodiversification and clade appearance remain uncertain. To resolve this, we interrogate an interval from ~527 to 519 Ma, encompassing multiple proposed global oceanic oxygenation events. We integrate the spatial and temporal distribution of shallow water, in situ reef metazoans, and trilobites, with high-resolution multi-proxy redox data through the highly biodiverse Siberian Platform. We document primarily dysoxic water column conditions, suggesting that early Cambrian metazoans, including motile skeletal benthos, had low oxygen demands. We further document oxygenation events coincident with positive carbon isotope excursions that led to modestly elevated oxygen levels. These events correspond to regional increases in species richness and habitat expansion of mainly endemic species, offering a potentially globally applicable model for biodiversification during the Cambrian Radiation.

INTRODUCTION

The Ediacaran to Cambrian rise of animals (metazoans) was a fundamental event in the history of life, expressed by the canonical Cambrian Radiation [~539 to 515 million years ago (Ma)], which records the apparently rapid appearance and diversification of modern metazoan body plans and ecologies (Fig. 1C) (*1*). A causal relationship between increasing shallow marine oxygenation and the Cambrian Radiation has long been proposed (*2*), but it is not clear whether oxygen availability rose progressively through this interval (*3*, *4*) and, if so, how this promoted biotic innovation and the radiation of early metazoans.

Models for the early Cambrian suggest atmospheric oxygen concentration of ~5 to 10% [~24 to 48% of the present atmospheric level (PAL)] (*5*), which would have created shallower and more dynamic redoxclines than found in modern oceans, along with the widespread occurrence of oxygen minimum zones along productive continental margins (*6*, *7*). Carbonate carbon ($\delta^{13}C_{carb}$), carbonate-associated sulfur ($\delta^{34}S_{CAS}$), and uranium ($\delta^{238}U_{carb}$) isotope compilations have been used to infer that Ediacaran-Cambrian oxygen levels were highly dynamic, with multiple ocean oxygenation events (OOEs) occurring globally over 1- to 10-Myr timescales (*8*–*11*).

There is a statistically significant antithetic relationship between the marine $\delta^{13}C_{carb}$ and $\delta^{238}U_{carb}$ records throughout the late Ediacaran to lower Cambrian interval (Fig. 1, A and B) (*12*). These co-occurring trends suggest that OOEs were linked to the dynamics of the global carbon cycle. The available data, while discontinuous, also suggest a baseline $\delta^{238}U_{carb}$ trend toward more positive values through the Ediacaran to mid-Cambrian interval (~580 to 515 Ma), which may indicate a progressive increase or stabilization of environmental oxygen, but this was punctuated dynamically by OOEs and anoxic episodes (*12*). Pulsed shallow marine OOEs, as inferred from $\delta^{238}U_{carb}$, $\delta^{34}S_{CAS}$, and $\delta^{13}C_{carb}$ records, occur at $\delta^{13}C_{carb}$ maxima and throughout the subsequent falling limbs in $\delta^{13}C_{carb}$ profiles (*11*–*13*). Here, falling $\delta^{13}C_{carb}$ and $\delta^{34}S_{CAS}$ reflect progressive oxygenation of the deeper water column, resulting in decreasing organic carbon and pyrite burial (*13*), consistent with coeval increases in $\delta^{238}U_{carb}$. Conversely, rising limbs in $\delta^{13}C_{carb}$ and $\delta^{34}S_{CAS}$ profiles (and falling $\delta^{238}U_{carb}$) reflect marine deoxygenation conducive to the progressive burial of organic carbon and pyrite, which leads to gradual atmospheric oxygenation (*13*). Thus, trends in each isotope system reflect global environmental oxygen availability, ultimately linked to the long-term carbon and sulfur cycles.

However, while these proxy systems can reveal trends in global environmental oxygenation, they do not inform ambient oxygen availability in regional shallow marine environments, where most early metazoans lived, and are also not sensitive to regional redox variability, especially on short timescales. Therefore, other regional redox proxy systems are necessary to infer more precise levels of oxygen and ecosystem habitability. Moreover, the biotic evolutionary response to redox change, as well as regional heterogeneity, can only be understood if local geochemical proxies are combined with local biotic data.

There has been much debate as to the actual drivers of an evolutionary response to oxygenation. Rising oxygen levels (potentially driven by increased productivity and organic matter burial) may have deepened the redoxcline, thereby extending habitable water depths (*14*). Enhanced oxygenation may also have enabled the evolution of more metabolically costly ecologies such as mobility and carnivory (*15*), as well as the ability to produce skeletal hard parts, thus promoting animal-sediment mixing [e.g., (*16*)] and evolutionary escalation (*17*). Conversely, the presence of shallow marine anoxia itself might have formed physical barriers to dispersal (*18*), and, thus, dynamic redox variability over evolutionary timescales may have promoted reproductive isolation and speciation (*19*).

The early Cambrian record of the Siberian Platform shows that phases of increased biodiversity, ecosystem complexity, and individual body sizes of reef-associated archaeocyath sponges and other metazoans synchronously coincided with the expansion of reef habitats on the shallow marine shelf (*14*, *20*). These biotic changes coincide with

[1]School of GeoSciences, University of Edinburgh, James Hutton Road, Edinburgh EH9 3FE, UK. [2]Borissiak Palaeontological Institute, Russian Academy of Sciences, Profsoyuznaya Street 123, Moscow 117647, Russia. [3]School of Earth and Environment, University of Leeds, Leeds LS2 9JT, UK. [4]Department of Palaeobiology, Swedish Museum of Natural History, Box 50007, Stockholm SE-10405, Sweden.
*Corresponding author. Email: Ruaridh.Alexander@ed.ac.uk

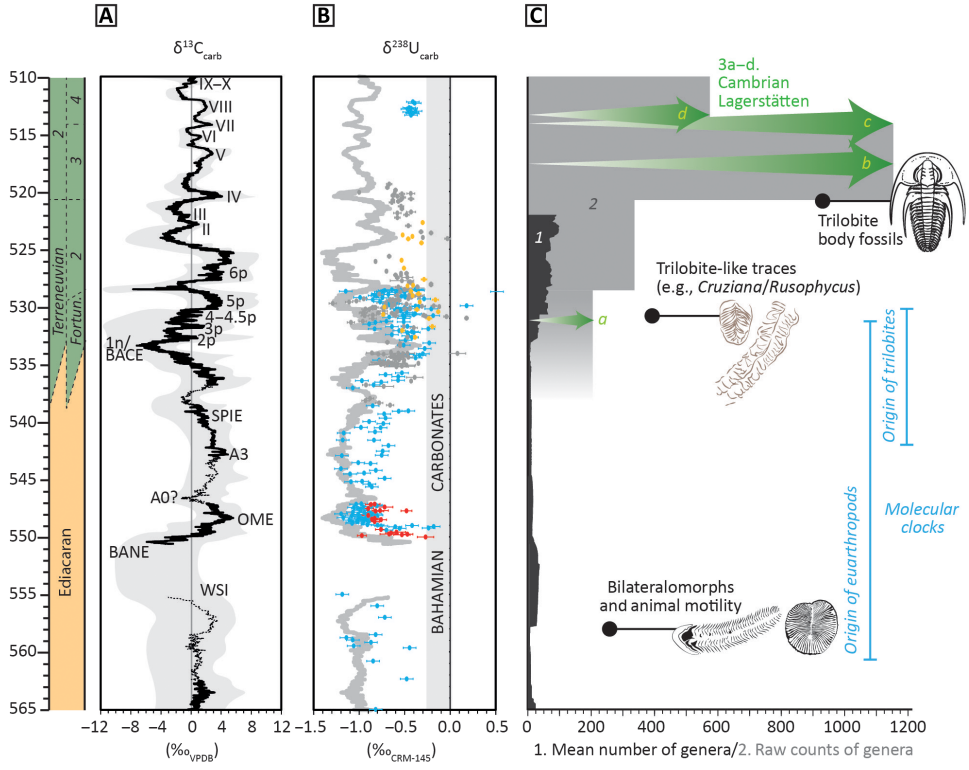

Fig. 1. Carbon and redox cycles with reconstructed metazoan biodiversification. (**A**) Global composite $\delta^{13}C_{carb}$ curve with uncertainty. (**B**) Temporally calibrated carbonate U isotope ($\delta^{238}U_{carb}$) data from multiple sources. Data are color-coded on the basis of region (blue, South China; gray, Siberia; red, Kalahari craton; yellow, Morocco). The oscillating pale gray line shows an inverted representation of the 10-point moving average of global $\delta^{13}C_{carb}$ data (A), used as a visual aid to show how a perfect anticorrelation between $\delta^{13}C_{carb}$ and the most reliable $\delta^{238}U_{carb}$ data would appear. (**C**) Reconstructed skeletal metazoan generic richness [1; from (*12*)] and frequency of genera per Cambrian stages [2; (*161*)]; origin of euarthropods (*162*) and trilobites (*26*) inferred from molecular clocks; first appearance of bilateralomorphs, trilobite-like trace fossils (*12*), and trilobite body fossils (*26*). Example Cambrian Lagerstätten: a, Kuanchuanpu; b, Chengjiang; c, Sirius Passet; d, Sinsk and Emu Bay Shale. Modified from (*12*).

positive carbonate-carbon isotope ($\delta^{13}C_{carb}$) peaks, reflecting carbon cycle perturbations and implying a (possibly transient) deepening of the redoxcline associated with each OOE (*12*–*14*). These intervals also coincide with increased rates of speciation during major sea-level lowstands, which may have permitted extensive oxygenation of shallow waters over the entire craton, providing oxic corridors for dispersal and the creation of new founder communities (*19*). Cambrian oxygen levels and their variability have not, however, been constrained by local paleoproxy data, and to trace the oxygen requirements of Cambrian metazoans necessitates the integration of local redox data with in situ, rather than reworked, fossil fauna (*21*, *22*).

While a rise in oxygen levels has been suggested to facilitate the evolution of costly ecologies [e.g., (*15*)], it does not offer a definitive mechanism for the origination of new clades or the appearance of key evolutionary innovations, such as a biomineralization, bilaterality, and segmentation, but may rather provide a viable mechanism by which existing metazoan clades are able to expand their habitat range and so diversify (Fig. 1C). The appearance of bilaterians required the formation of new mechanisms to coordinate multiple cell types and an expanded capacity to coordinate gene activities to generate new tissues and organs. However, how much developmental capacity was present in the last common ancestor of protostomes and deuterostomes, and how much arose independently in major clades, remains unclear (*23*). New spatial and temporal regulatory hierarchies enabled widespread co-option events in metazoans, possibly during the late Ediacaran, that allowed the independent appearance of many key metazoan innovations such as skeletons, segmentation, a nervous system and head, appendages, sensory systems, and a regionalized gut (*23*). These are the hallmark of the Cambrian Radiation, and such a rapid and independent acquisition of different, novel characters in many different clades implicates possibly numerous external triggers (*23*).

All clades predate their first appearance of macroscopic representatives in the fossil record, which offers only a minimum estimate age for the clade (*24*, *25*). This is not only due to vagaries of preservation, sampling, and acquisition of taxonomically identifiable features but also suggests that the developmental and morphological novelties required to define a new clade are decoupled from the ecological and/or extrinsic drivers and their feedbacks that allowed these clades to proliferate and, hence, rise to ecological prominence in the fossil record. For example, molecular clocks suggest that the euarthropods may have appeared in the latest Ediacaran and trilobites in the Fortunian (broadly coincident with trilobite-like traces); however, trilobite body fossils did not appear until 521 Ma, after which they underwent a rapid radiation, i.e., an increase in species richness accompanied by morphological diversification (Fig. 1C) (*26*). In other words, developmental capacity is decoupled from morphologic complexity, and the developmental capacity that early metazoans had was not realized and promoted until subsequent environmental (such as oxygen

or productivity) and/or ecological (such as competition and macropredation) changes occurred, which together characterized and fueled the early Cambrian Radiation (*23*).

Here, we present an integrated, high-resolution early Cambrian record from ~527 to 519 Ma (Cambrian stages 2 to 3, Tommotian-Atdabanian), constrained within a chemostratigraphic age model of globally established and correlated $\delta^{13}C_{carb}$ oscillations (from cycles 6p/7p to IV) (*27*), to understand potential relationships between the Cambrian Radiation and associated water column redox conditions. We combine major element and multiple paleoredox proxy data, including Fe speciation, redox-sensitive trace elements, and I/(Ca + Mg) ratios, with skeletal metazoan distributions and metrics of diversification, from three broadly coeval shallow water localities on the biodiversity hotspot of the lower Cambrian Siberian Platform (Fig. 2A). These data constrain the oxygen demands of early Cambrian skeletal metazoans and inform the drivers of the Cambrian Radiation coincident with the global appearance and diversification of trilobites, representing one of the earliest, major motile and skeletal groups.

Geological background

The Siberian Platform formed a vast tropical continent (Fig. 2B) with several episodically isolated carbonate banks/platforms (Fig. 2A) (*28*, *29*) that housed over a third of all known skeletal taxa from the early Cambrian (*13*). The Siberian fauna diversified through the early Cambrian (Fig. 3G), with the total number of fossil-bearing sites increasing from 25 to 46 and expanding in geographical area through $\delta^{13}C_{carb}$ peaks II and III (~523 to 522 Ma, stage 2, middle Tommotian; Fig. 3 and table S6). The $\delta^{13}C_{carb}$ peak IV (~521 to 520 Ma, stage 3, early Atdabanian) coincides with a major sea-level lowstand (Fig. 3, A and B) and also with an acme of metazoan biodiversity (Fig. 3G) (*14*, *20*), high rates of overall origination (Fig. 3H), archaeocyath speciation and endemism (*14*) (Fig. 3I), and the global appearance and rapid diversification of trilobites (Fig. 3J and table S7) (*30*–*33*).

Here, we interrogate the biotic and geochemical record of three geographically disparate sites on the Siberian Platform: Selinde River, Sukharikha River, and Ulakhan-Ald'yarkhay Brook (Fig. 2A). Samples from the Selinde River section (Aldan-Lena carbonate platform, SE Siberian Platform) record the longest temporal interval, from $\delta^{13}C_{carb}$ excursion 6p/7p (~527 Ma) to after $\delta^{13}C_{carb}$ peak IV (~519.5 Ma) (Fig. 2A and figs. S1 and S2), but those from the Sukharikha River (Igarka carbonate bank, NW Siberian Platform) and the Ulakhan-Ald'yarkhay Creek at the Khara-Ulakh Mountains (Anabar-Lena carbonate platform, NE Siberian Platform; Fig. 2A) broadly cover the $\delta^{13}C_{carb}$ peak IV interval only (Fig. 3A and figs. S1 and S2), with Sukharikha occupying a slightly deeper bathymetric position (see the Supplementary Materials) (*28*, *34*). These successions alone record diverse biotas of >100 species (Fig. 3) of mostly reworked small shelly fossils (SSFs), in situ archaeocyath sponge reefs, and the first trilobites (both in situ and slightly reworked), which appear coincident with $\delta^{13}C_{carb}$ peak IV (see the Supplementary Materials; Fig. 3J, fig. S1, and table S5). This association of the $\delta^{13}C_{carb}$ and metazoan fossil records is found throughout many other sections on the Siberian Platform (*13*, *27*, *35*).

RESULTS

Low oxygen levels and oscillations in the early Cambrian

Our multi-proxy approach allows a detailed assessment of the redox evolution on the Siberian Platform (see Materials and Methods for methods and geochemical framework, and tables S1 to S5 for all data). Samples with iron concentrations >0.5 wt% (*36*) were analyzed for total iron/aluminum (Fe_T/Al), highly reactive/total iron (Fe_{HR}/Fe_T), and pyrite-bound iron/highly reactive iron (Fe_{py}/Fe_{HR}) ratios (Fig. 3, C and D, and fig. S1H). At Selinde, Fe_T/Al ratios are consistently above the calibrated anoxic threshold (0.66) (*36*) through the lower part of the section, followed by fluctuations to lower values in the uppermost Tommotian and lower Atdabanian (Fig. 3C). Fe_{HR}/Fe_T ratios are generally consistent with Fe_T/Al ratios, with values above the anoxic threshold [0.38; (*37*)], with the exception of some samples that fall in the equivocal zone in the uppermost Tommotian (Fig. 3D). Fe_{py}/Fe_{HR} ratios are all low (fig. S1H), indicating negligible

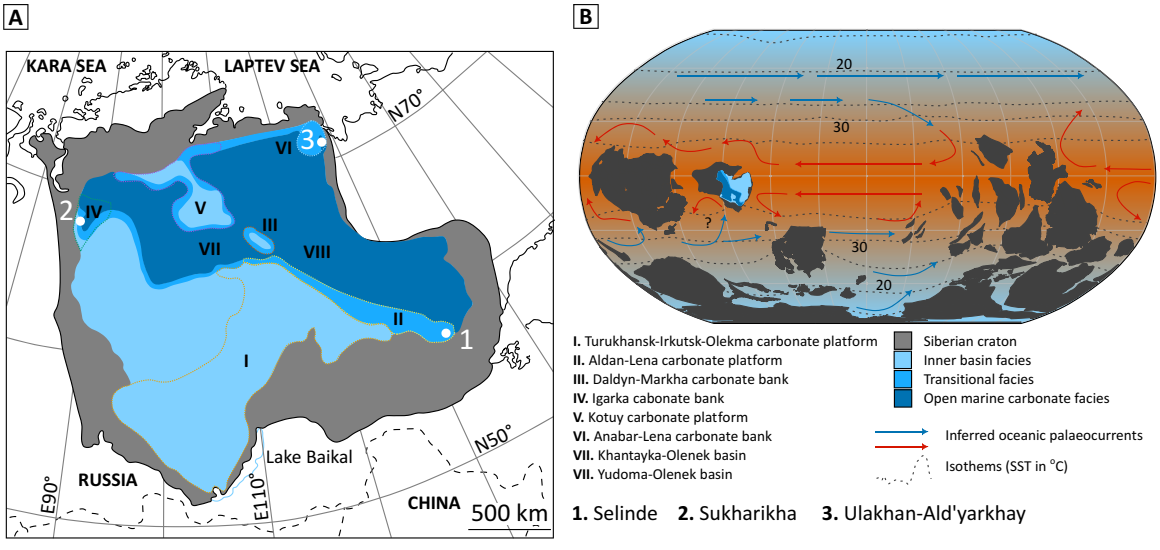

Fig. 2. Early Cambrian of the Siberian craton. (**A**) Paleofacies map of Cambrian stages 2 to 3 (~529 to 514.5 Ma) showing the distribution of six banks/platforms (I to VI) and the study sites (1 to 3) [after (*28*)]. (**B**) Cambrian paleogeography at 521 Ma [after (*47*, *163*)] with position of the Siberian craton and possible ocean currents. Modeled sea surface temperature and isotherms [after (*48*)].

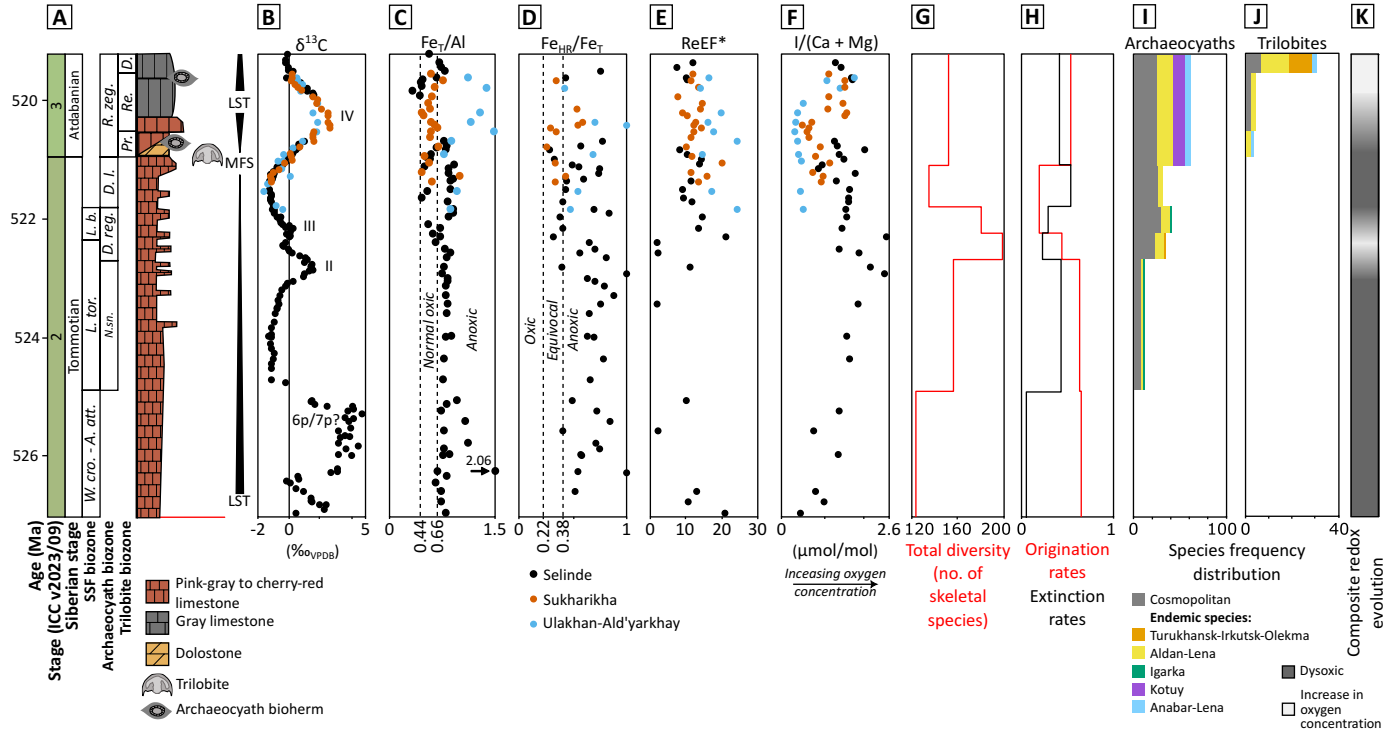

Fig. 3. Summary of redox data and metazoan dynamics through the early Cambrian on the Siberian Platform. (**A**) Composite stratigraphy [after (*28*, *164*–*166*)]. MFS, maximum flooding surface. LST, lowstand systems tract. Siberian biozone subdivision after (*19*) and references therein. (**B**) C isotope ($\delta^{13}C_{carb}$) record [from (*75*, *166*, *167*)] with the first appearance of trilobites and archaeocyath reefs. (**C**) Fe_T/Al. (**D**) Fe_{HR}/Fe_T ratios. Dashed lines in (C) represent the empirically derived normal oxic range (*36*). Dashed lines in (D) represent the empirically derived normal oxic and anoxic thresholds with an equivocal zone between (*37*). (**E**) Re enrichment factors (ReEF*). (**F**) I/(Ca + Mg). (**G**) Total diversity on the Siberian Platform from (*59*). (**H**) Rates of origination and extinction of skeletal species on the Siberian Platform (*59*). (**I**) Distribution of cosmopolitan and endemic species of all archaeocyath sponges on the Siberian Platform (*19*). (**J**) Distribution of cosmopolitan and endemic species of trilobites on the Siberian Platform (see table S7). (**K**) Reconstructed composite redox evolution.

free sulfide in the water column and during diagenesis (*37*). At Sukharikha, most Fe_T/Al and Fe_{HR}/Fe_T values fall below the anoxic threshold, with occasional elevated values, while low Fe_{py}/Fe_{HR} ratios again indicate limited sulfide production. At Ulakhan-Ald'yarkhay, Fe_T/Al and Fe_{HR}/Fe_T ratios consistently fall above the anoxic thresholds, with low Fe_{py}/Fe_{HR} ratios.

The common occurrence of enrichments in Fe_T/Al and Fe_{HR}/Fe_T ratios indicates at least periodic anoxic mobilization of Fe^{2+} and subsequent precipitation, while low Fe_{py}/Fe_{HR} ratios suggest limited production of sulfide, even during diagenesis. However, this does not necessarily mean that the overlying water column was anoxic since upwelling of anoxic-ferruginous deeper waters into better ventilated shallower waters would result in precipitation of Fe^{2+} and hence Fe enrichments in the sediment (*38*). Thus, to provide further insight into redox conditions at the site of deposition, we use a refined approach for calculating enrichment factors (termed EF^*) for redox-sensitive trace metals (e.g., U, Mo, and Re) in carbonate-rich lithologies (see Supplementary Materials) (*39*). Resultant EF^* values for U and Mo are typically low at all three sites (~1; figs. S2F and S3 and tables S2 and S3), indicating essentially no enrichment in either element, and, hence, anoxia was apparently not prevalent at the site of deposition (*40*). By contrast, all sections are highly enriched in Re (Fig. 3E and fig. S2H). Re has a higher reduction potential than U and Mo and begins to accumulate in sediments under dysoxic conditions [dysoxic conditions being defined as ~8.8 to 88 μmol/kg O_2, or 9 to 89 μM; (*41*)] at the sediment-water interface (*42*). Hence, given that Sukharikha and Ulakhan-Ald'yarkhay are distal from continental input, our combined data are consistent with dysoxic conditions on the Siberian Platform, which promoted oxidation of Fe^{2+} in upwelling anoxic-ferruginous deeper waters.

We further measured I/(Ca + Mg) ratios to potentially reveal more subtle variations in oxygen availability at each site and through time. The data show no significant correlation with either total organic carbon or stable oxygen isotopes ($\delta^{18}O$) (figs. S4 to S6), implying minimal influence of organic matter or diagenesis on iodine concentrations. I/(Ca + Mg) ratios are low at all sites, relative to the typical "oxic" threshold of ~2.6 μmol/mol (*43*, *44*): Selinde (0.42 to 2.50 μmol/mol, mean = 1.47 μmol/mol), Sukharikha (0.47 to 1.56 μmol/mol, mean = 1.02 μmol/mol), and Ulakhan-Ald'yarkhay (0.29 to 1.73 μmol/mol, mean = 0.65 μmol/mol) (Fig. 3F), suggesting limited iodide oxidation within the water column at the depth of carbonate formation (*45*). Such values suggest that oxygen levels were low and predominantly conducive to iodate reduction (i.e., the water column was likely manganous to nitrogenous). Carbonate I/(Ca + Mg) ratios of <2.5 μmol/mol (equivalent to IO_3^- < 0.25 μM in seawater) indicate seawater [O_2] of <20 to 70 μM in modern and ancient oceans (*44*, *46*) and are thus consistent with our interpretation of prevalent dysoxia on the platform. These data are consistent with modeled shallow marine O_2 concentrations throughout the early Palaeozoic (*4*). However, Selinde records the highest average ratios and Ulakhan-Ald'yarkhay records

the lowest (Fig. 3F), implying a meaningful difference in oxygen concentrations between each of these sections and thus spatial variability in oxygen concentrations across the platform. In sum, our data reveal that Selinde was generally better oxygenated in the upper half of the section, but across $\delta^{13}C_{carb}$ peak IV, [O_2] was progressively depleted from Sukharikha to Ulakhan-Ald'yarkhay (Fig. 3F).

While our geochemical data necessarily represent time-averaged concentrations of homogenized samples (and hence integrate short-term variability), the stratigraphic trends in I/(Ca + Mg) ratios can be attributed to longer-term changes in relative oxygen concentrations (at levels sufficient to oxidize iodide) at the locus of carbonate mineral formation. I/(Ca + Mg) ratios at Selinde progressively increase through the lower half of the section to peak values broadly coincident with $\delta^{13}C$ peaks II and III before falling to intermediate values, while ratios at Sukharikha and Ulakhan-Ald'yarkhay increase after peak IV, coincident with the sedimentation occurring in the shallowest waters (Fig. 3, A and F). Despite overall dysoxic conditions, I/(Ca + Mg) ratios therefore indicate the development of better oxygenated conditions coincident with $\delta^{13}C$ peaks II, III, and after peak IV. Samples that show a progressive increase in I/(Ca + Mg) ratios in the lower half of the section at Selinde also show persistently elevated Fe_{HR}/Fe_T ratios, but during the interval of sustained intermediate values at Selinde and Sukharikha (i.e., between $\delta^{13}C$ peaks III and IV), Fe_{HR}/Fe_T ratios fluctuate to values that are sometimes in the equivocal zone, supporting unstable but overall better oxygenated conditions. These data support the hypothesis that the Siberian Platform was primarily dysoxic, but with transient intervals of moderately enhanced oxygenation over $\delta^{13}C$ peaks II, III, and IV. Oxygen levels during these better oxygenated intervals remained, however, at relatively low levels.

DISCUSSION

A shallow redoxcline limited habitable space

Our combined paleoredox data provide the first independent confirmation that oceanic oxygen levels remained low in the early Cambrian even within densely populated and biodiverse marine basins. Notwithstanding possible diagenetic effects (see Materials and Methods, Redox proxy systematics section), the low I/(Ca + Mg) values are consistent with all other proxy data, including redox-sensitive trace metal EFs. Our data also show modest, regional shallow marine oxygenation on the Siberian Platform coincident with major, and globally correlatable, positive $\delta^{13}C_{carb}$ excursions, thereby supporting the hypothesis that these events represent global shallow marine OOEs (*13*). On the basis of available I/(Ca + Mg) data, the general levels of oxygenation appear to have been broadly similar, but possibly slightly elevated, to those recorded in some terminal Ediacaran (550 to 539 Ma) carbonate environments (*46*).

Our data, however, strongly suggest that OOEs were unlikely to have established pervasively oxic conditions below reef margins, and the redoxcline was therefore very shallow and dynamic, significantly defining and limiting habitable space. Deeper ferruginous waters were apparently present off the platform margin, with episodes of dynamic oceanic upwelling resulting in elevated Fe_{HR}/Fe_T values in shallow marine settings, despite locally dysoxic conditions (Fig. 4) (*18*). Potential ocean circulation dynamics based on a recent global plate reconstruction (*47*) and modeled Cambrian oceanic surface temperatures (*48*) suggest that the southwest margin of the platform (the region of Ulakhan-Ald'yarkhay) may have been a site of nutrient upwelling and potentially anoxic waters (Fig. 2B) (*19*) but with upwelling precluded by the presence of the Kolyma-Omolon terrain on the present-day eastern margin of the platform (Fig. 4) (*49*, *50*). Upwelling of nutrients would have sustained high primary productivity in this region and reduced oxygen availability in the vicinity of upwelling relative to coeval sections on the platform. Given the similarity in the I/(Ca + Mg) trends at Sukharikha and Ulakhan-Ald'yarkhay, it is likely that they were both in close proximity to the open ocean and the influence of productivity-driven anoxic waters to the south (Fig. 4), with the higher I/(Ca + Mg) ratios at Selinde likely reflecting its more distal setting from anoxic waters and the open ocean.

Metazoan habitat expansion and diversification in response to oxygenation events

Combining local redox data with the temporal and spatial distribution of metazoans on the Siberian Platform reveals the biotic response

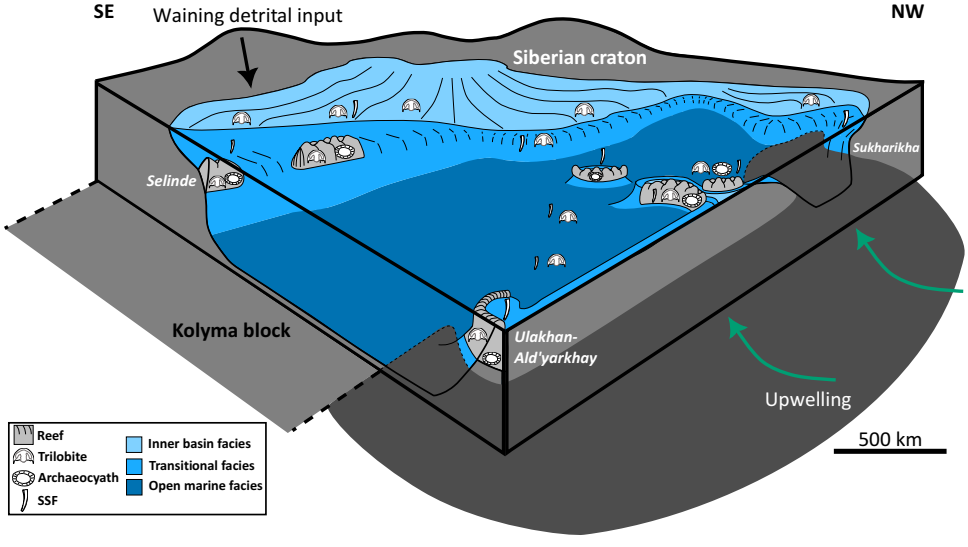

Fig. 4. Block diagram summarizing the spatial redox and metazoan distribution on the Early Cambrian Siberian Platform. Paleofacies after (*28*); SSF distribution after (*58*); archaeocyath sponge distribution after (*19*); trilobite distribution after (*31*, *58*).

to oxygenation. Sukharikha shows a low overall biodiversity (i.e., species richness) and an absence of archaeocyath reefs in early stage 3 (fig. S1 and table S5), consistent with its deeper position and the influence of proximal anoxic waters. Although overall metazoan biodiversity during the same interval is high at Selinde, this consists mostly of SSFs (mainly hyoliths). These are generally slightly reworked (i.e., derived from the same sedimentary setting in which they were deposited) in the upper part of this section (beds 24 to 54) (fig. S1). Only three reef-associated archaeocyath sponges and five trilobite species are in situ (fig. S1). Metazoan reefs (with associated SSFs and trilobites) are recorded before peak IV at Ulakhan-Ald'yarkhay (Unit 6; fig. S1), suggesting that they were established before those at Selinde, which is also consistent with the shallower bathymetric position of Ulakhan-Ald'yarkhay (see the Supplementary Materials). A reworked fossil assemblage is preserved in limestone units below these reefs, but few fossils are preserved after $\delta^{13}C_{carb}$ peak IV (fig. S1). Our paleoredox data indicate that these metazoan reefs grew under dynamic, primarily low-oxygen backgrounds before an increase in oxygen concentrations after $\delta^{13}C_{carb}$ peak IV, and were thus either adapted to low-oxygen conditions or potentially colonized the sea floor during relatively short-lived higher-oxygen conditions but aliased by time-integrated sample homogenization [e.g., (*21*, *22*)].

At the base of the Selinde section (beds 15 to 23), marked by a transgressive surface, SSFs are by contrast more variably reworked, including those derived from other sedimentological settings, and preserved as casts replaced by glauconite and phosphate. High generic diversity during this interval may be due to the concentration of reworked skeletal fossils at the base of transgressive lags (*12*). Both early glauconitization and phosphatization are indicative of replacement under variable porewater redox conditions conducive to intense Fe-P cycling (*51*–*53*). Such replacement also tends to be associated with low sedimentation rates, stratigraphic condensation, and reworking (*54*–*56*). The unusually high abundance of authigenic glauconite in the Cambrian (*57*) indicates that these porewater redox oscillations occurred near the sediment/water interface, requiring low-oxygen and fluctuating conditions at or near the seafloor. The high abundance of glauconitized and phosphatized SSFs therefore supports the hypothesis that dynamic, low-oxygen conditions were pervasive on the Siberian Platform. While our data are in agreement with this, fluctuations in oxygen concentrations responsible for early glauconitization and phosphatization likely occur on even shorter timescales than our dataset is able to capture, further indicating highly dynamic redox conditions.

Other sites on the Siberian Platform that are characterized by a high abundance of fossils were also restricted to the shallowest settings, representing deposition at water depths within fair-weather wave to storm-wave base (see the Supplementary Materials) (*19*, *58*). Fossil distributions throughout these sections suggest, then, that lower-oxygen conditions in deeper waters restricted most skeletal metazoans to shallow, bank tops where oxygen concentrations were sufficiently high, and potentially enhanced by physical ventilation mechanisms, throughout $\delta^{13}C$ peak 6p/7p and across peaks II and III.

Archaeocyath sponges diversified and underwent habitat expansion around $\delta^{13}C$ peaks II, III, and IV (~521 to 520 Ma, early Atdabanian) (Figs. 3I and 5) (*19*). Trilobites appear and diversify before and during peak IV (*59*) from three genetically distinct populations. Species of the genus *Profallotaspis* (superfamily Fallotaspidoidea) first appear in the *Profallotaspis jakutensis* biozone and increase in diversity to 31 species in the *Delgadella anabara* biozone (Figs. 3J and 5 and table S7). On the basis of our paleoredox proxy data, $\delta^{13}C$ peaks II, III, and IV can be interpreted as moderate OOEs that punctuated pervasively low-oxygen environments.

This diversification was accompanied by marked habitat expansion. Archaeocyaths notably expanded their ranges from the Aldan-Lena area to the Turukhansk-Irkutsk-Olekma and Kotuy carbonate platforms and the Daldyn-Markha carbonate bank (Fig. 3I) (*19*). Between peaks III and IV, archaeocyath geographic distribution contracted and only 32 species survived on the Aldan-Lena platform in the latest Tommotian, of which only five were endemic (*19*). During the peak IV interval, archaeocyaths again expanded their range to form endemic faunas in the Kotuy and Anabar-Lena banks (Fig. 3I) (*19*). Similarly, by the end of the peak IV interval, trilobites had diversified and extended their habitats after their first appearance (fallotaspidoids) in the reef settings of the Aldan-Lena (including Selinde) and Anabar-Lena (including Ulakhan-Ald'yarkhay) banks. They began to colonize the shallow calcareous-dolomitic muds of the inner Turukhansk-Irkutsk-Olekma basin (superfamillies Corynexochoidea and Redlichioidea) and the argillaceous-calcareous muds of the deeper Yudoma-Olenek and Khantayka-Olenek basins (the smallest species represented by the Family Hebediscidae and Superfamily Ellipsocephaloidea) (Figs. 3J and 5 and table S7), thus creating three distinct trilobite paleocommunities (*31*). Colonization of the previously unhabitated Turukhansk-Irkutsk-Olekma basin was the result of the apparently rapid appearance of numerous, short-lived endemic species (Figs. 3J and 5 and table S7).

During the peak IV interval, synchronous expansions of both diversity and habitat found in both archaeocyaths and trilobites coincident with an episode of oxygenation also occurred during a sea-level lowstand (Figs. 3A and 5). While archaeocyaths appear to have diversified before trilobites, beginning during the rising limb of $\delta^{13}C_{carb}$ peak IV, this may not be the case due to possible aliasing of data. Trilobite fossil occurrences can be binned according to three relatively short-lived biozones, allowing a more precise stratigraphic placement within the peak IV interval (Fig. 3J), but archaeocyath data can only be placed within one biozone over the same interval (Fig. 3I). It is therefore not possible to determine whether the greatest increase in archaeocyath diversity and habitat expansion occurred before, during, or after peak IV. Regardless, these data support the hypothesis that when an OOE coincided with relatively low sea-level, this coupled environmental change promoted more extensive oxygenation of shallow waters over the entire craton, thus providing oxic corridors for dispersal and the creation of new founder communities (*19*). This is supported by the marked increase in both archaeocyath and trilobite diversity and habitat expansion during this interval (Figs. 3, I and J, and 5, C and D; and table S7).

We conclude that during the Cambrian Radiation, from ~528 to 519 Ma, the Siberian Platform was characterized by low-oxygen conditions, with a dysoxic water column in shallow marine depositional environments where metazoans lived. Our suggestion that early Cambrian metazoans, even mobile, calcified bilaterians such as trilobites, did not have high oxygen demands is supported by modern ecophysiological data indicating that all of the critical oxygen thresholds of function and ecology, including high-energy lifestyles, can be met at low oxygen levels [equating to ~22 μM or 8% of modern surface ocean levels; Fig. 3D (*60*)]. In the modern ocean, metazoans with the energetically costly lifestyle of carnivory may occur at very low oxygen concentrations (~0 to 9 μM), but the diversity of species increases with increasing oxygen concentrations with peak diversity being achieved from ~22 to 45 μM (*15*, *60*). It is possible, however, that even the modest oxygenation events discerned

here may have moved metazoans past critical ecological thresholds that further facilitated diversification.

Adaptation to low oxygen levels is suggested to have been an ancestral character of several groups, including trilobites, which appear to have had the respiratory proteins and gill structures to cope with low oxygen levels (*61*, *62*). The upper limb branches of Cambrian biramous arthropods (including corynexochide and olenide trilobites) had dumbbell-shaped filaments, which would have overcome the limited effectiveness of the distributed system of cuticular diffusion found in small-sized animals (*62*). If early fallotaspidoid trilobites had relatively short carapaces with long pleurae, this would have allowed these forms to extend filament height and gill shaft length, thus maximizing the respiratory surface area and maintaining oxygen intake at higher levels, similar to some extant crustaceans inhabiting oxygen-depleted waters (*63*). Such morphologies might explain the extensive distribution of hebediscid trilobites over the Siberian Platform (Fig. 5) (*64*). Furthermore, modern sponges can tolerate oxygen levels of <4% PAL (*65*, *66*), and the slow, motile gastropods *Patella* spp. and *Haliotis fulgens*, which both belong to ancient lineages, are able to decrease their oxygen demands under hypoxia (*67*, *68*). Predatory chaetognaths, as represented by protoconodonts (*69*, *70*), have an efficient diffusive respiratory system given their small size, although they lack gills (*71*). It is possible, however, that many other early Cambrian metazoans may have had inefficient respiratory systems, potentially explaining the small size of Cambrian SSFs [not ≥80 mm but most <30 mm; (*20*, *72*–*75*)] compared to Ordovician representatives of the same groups, which were one to two orders larger (*76*, *77*).

Toward a global model

The origin of major metazoan clades always predates the appearance of their first macroscopic representatives in the fossil record, and while environmental changes and ecological feedbacks may have been required to realize their developmental capacities, it is not yet clear whether these relate to any changes in ambient oxygen levels. Increases in oxygen availability may, however, have enabled metazoans to take advantage of both developmental potential and ecological opportunities subsequent to the establishment of a major group. Here, we show that increases in oxygen concentrations may have provided a viable mechanism by which existing groups were able to expand their habitat range and hence diversify, which was perhaps enhanced by reaching critical ecological thresholds. This is often accompanied by morphological and ecological diversification of these clades. However, our data show that high oxygen levels were not required for Cambrian metazoan diversification and radiation. Against the backdrop of low-oxygen conditions, pulsed, but only modest, increases in shallow marine OOEs facilitated an increase in species richness via habitat expansion in archaeocyath sponges and trilobites, which occurred approximately coincident with global $\delta^{13}C_{carb}$ maxima recorded by peaks II, III, and IV. It was these dynamic, but consistently low, oxygen conditions within shallow marine environments, combined with cycles of geographical isolation and

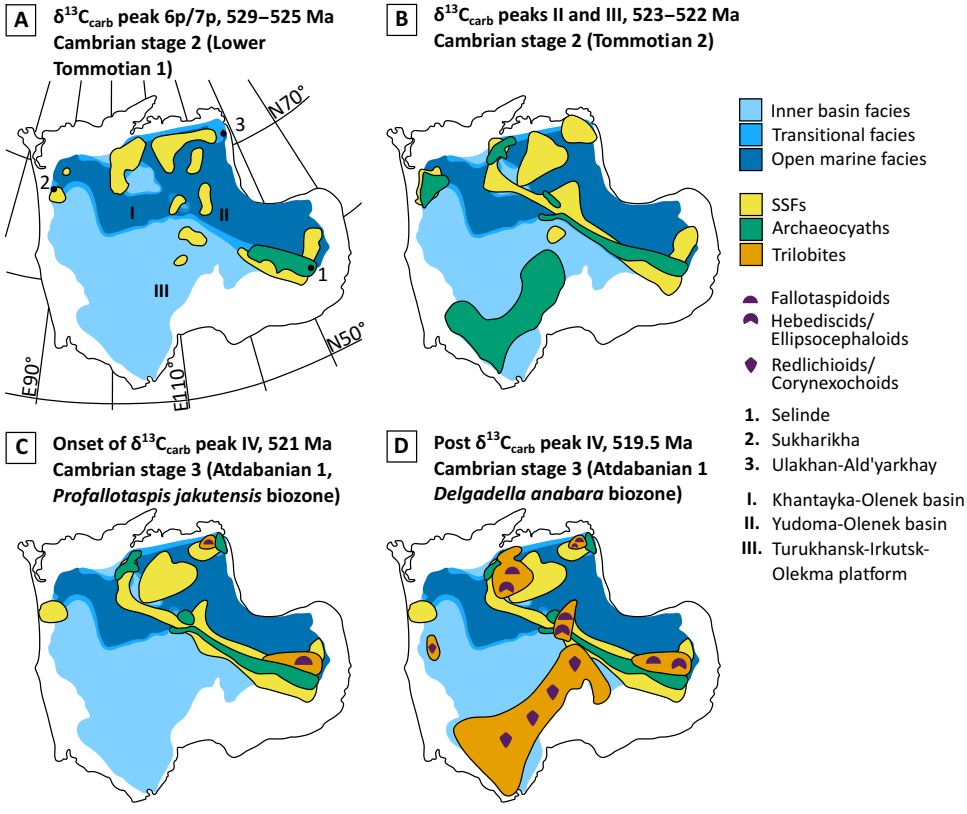

Fig. 5. Metazoan temporal and spatial distribution on the early Cambrian Siberian Platform, from 529 to 519.5 Ma. (**A**) Cambrian Stage 2, 529-525 Ma. (**B**) Cambrian Stage 2, 523-522 Ma. (**C**) Cambrian Stage 3, 521 Ma. (**D**) Cambrian Stage 3, 519.5 Ma. Paleofacies after (*28*); SSF distribution after (*58*); archaeocyath sponge distribution after (*19*); trilobite distribution after (*31*, *58*).

expansion, that drove diversification in the important biodiversity hotspot of the Siberian Platform.

The synchronous nature of $\delta^{13}C_{carb}$ peaks and OOEs suggest that these likely record global redox dynamics (*12*), with oxygenation during peak IV potentially being further enhanced and more regionally extensive on the Siberian Platform due to its coincidence with a major sea-level lowstand. While this study, therefore, represents an integration of local paleoredox and biotic data, it creates a model that has a potentially wide application, as $\delta^{13}C_{carb}$ cycles are extensively documented from many regions and have been demonstrated to be globally synchronous (*12*, *78*). Our data are also consistent with models that infer global OOEs through the correlation and integration of the C, S, and U isotope systems (Fig. 1, A and B) (*11*–*13*). Similar integrative studies are required for other Cambrian successions to better constrain redox heterogeneity and its impact on diversification, and while other regions may show higher oxygen levels during global OOEs (during $\delta^{13}C_{carb}$ peaks), we argue that high-oxygen conditions are not required to explain the Cambrian Radiation.

MATERIALS AND METHODS

Sample preparation

Samples were halved with a diamond saw to retain archive material, and weathered surfaces were removed from one half. The samples were washed and dried at 40°C. Samples with visible signs of alteration and/or veining were rejected at this point. Halved samples were crushed and pulverized to homogeneous powder (<60 μm) using a tungsten carbide Tema laboratory disc mill.

Total digestion

After ashing at 550°C for 8 hours, the samples were quantitatively dissolved in trace metal grade HNO_3, HF, and $HClO_4$, heated in open polytetrafluoroethylene cups and left to dry fully over a period of 24 hours before the addition of H_3BO_3 to prevent the formation of Al complexes. Dry residues were then dissolved in concentrated HNO_3 and diluted with ultrapure 18 megohm H_2O. Major element concentrations were analyzed using inductively coupled plasma optical emission spectrometry (ICP-OES, Thermo Fisher Scientific iCAP 7400), and trace element concentrations were measured using ICP mass spectrometry (ICP-MS, Thermo Fisher Scientific iCAPQc) at the School of Earth and Environment, University of Leeds. Total digestions of a standard material (SBC-1, US Geological Survey) yielded values within the certified range for all elements analyzed (<4%).

Fe speciation

Iron speciation analyses follow the established method of (*79*), as modified in (*38*). An initial leach targeting iron bound in carbonate phases (Fe_{carb}) used Na-acetate, buffered to pH 4.5 with acetic acid and agitated at 50°C for 48 hours. This was followed by a 2-hour iron (oxyhydr)oxide (Fe_{ox}) extraction in Na-dithionite buffered to pH 4.8, and then a final extraction of magnetite (Fe_{mag}) with ammonium oxalate for 6 hours. All steps of the sequential leach were performed at the Cohen Laboratories, University of Leeds, and resultant solutions were analyzed for Fe using a Thermo Fisher Scientific iCE-3000 series flame atomic absorption spectrometer, with replicate extractions for each step yielding relative standard deviations (RSDs) of <5%. To ensure accuracy, Fe speciation reference material (WHIT) (*80*) was run alongside each batch.

The concentration of pyrite iron (Fe_{py}) was determined through a boiling chromous chloride [$Cr(II)Cl_2$] distillation with a pre-leach in boiling 6 M HCl for quantitative extraction of acid volatile sulfide (AVS). Pre-leaching confirmed that no AVS was present. Weight percent Fe_{py} was determined gravimetrically after stoichiometric precipitation of Ag_2S.

I/(Ca + Mg)

Measurement of I/(Ca + Mg) ratios followed the procedure of (*81*). One hundred milligrams of powder was washed with 18 megohm of H_2O and dried at 40°C for 48 hour. Five milligram of resultant powder was weighed for analysis. The samples were digested with 3% HNO_3. Iodine was stabilized with 3% ammonium hydroxide to create a mother solution. This was made to volume with a matrix solution of 3% HNO_3 + 0.5% ammonium hydroxide + 3% methanol. The solution was diluted with matrix to produce 50 ± 5 μg/ml Ca concentrations in each sample. Ca and Mg concentrations were measured using ICP-OES (Varian Vista Pro ICP-OES), and I concentrations were measured using ICP-MS (high-resolution single collector ICP-MS, AttoM) at the University of Edinburgh, using a Tellurium internal standard. JCP-1 coral standard was analyzed as a reference material with RSDs <4%.

Elemental EFs

EFs provide a quantification of the level of accumulation of redox-sensitive trace metals (*40*, *82*), and EFs are commonly calculated for siliciclastic sediments by the following

$$\text{Element}_{EF} = \frac{\text{Element} / \text{Al}}{\text{Element}_{UCC} / \text{Al}_{UCC}} \quad (1)$$

where UCC represents upper continental crust [here, we use concentrations in (*83*) except for Re, which is not reported, for which we use values in (*84*)]. However, using EF values in sediments rich in carbonates is problematic as low Al concentrations in such sediments result in elevated EFs relative to siliciclastic sediments (*85*). This may be navigated by calculating elemental excess concentrations (*39*), which are calculated by the following

$$\text{Element}_{excess} = \text{Element}_{sample} - \left(\text{Al}_{sample} \times \frac{\text{Element}_{UCC}}{\text{Al}_{UCC}} \right) \quad (2)$$

These values are then used to calculate revised EF values (EF^*) for carbonate-rich lithologies (*39*)

$$\text{Element}_{EF}{}^{*} = \frac{\text{Element}_{excess} / \text{Element}_{UCC}}{\text{Element}_{UCC}} \quad (3)$$

Using EF^* allows the assessment of elemental EFs in carbonate rocks and furthermore facilitates comparison to siliciclastic lithologies.

Redox proxy systematics

We deploy a multi-proxy approach to assess the redox evolution of the Siberian Platform. Fe speciation facilitates the assessment of redox conditions by measuring the concentration of Fe_{HR} (that is, a highly reactive Fe pool composed of Fe in carbonate and ferric oxide minerals, magnetite, and pyrite—Fe_{carb}, Fe_{ox}, Fe_{mag}, and Fe_{py}) and normalizing these data to Fe_T (the total concentration of Fe within a sample) (*37*, *79*). Fe speciation has been calibrated in a variety of modern and ancient settings and is able to constrain oxic and "anoxic" conditions (*37*, *38*, *86*), whereby ratios ≤0.22 are commonly indicative of oxic water column conditions. Ratios ≥0.38 are commonly indicative of

precipitation of Fe–bearing unsulfidized mineral phases and Fe sulfides under anoxic water column conditions in ferruginous and euxinic settings, respectively (*87*, *88*). These absolute thresholds may not be applicable to all depositional environments (e.g., high rates of deposition may obscure anoxic signals due to decreased Fe_{HR}/Fe_T values or mineral transformation during diagenesis), and, hence, an equivocal zone is defined between these thresholds (*37*). Fe_T/Al ratios may be used to further assess redox conditions in the case of obscured values due to diagenesis. Values >0.66 are indicative of deposition under anoxic waters, with a typical oxic range of 0.44 to 0.66 (*36*).

Anoxic ferruginous and euxinic conditions may be distinguished by the proportion of pyrite-bound Fe (Fe_{Py}) within the Fe_{HR} pool, whereby values >0.8 are indicative of deposition under a euxinic water column (*37*). The potential for addition of Fe_{HR} into carbonates during diagenesis means that care must be taken when analyzing carbonates for Fe speciation. Calibration of Fe speciation data from carbonates suggests that samples with $Fe_T > 0.5$ wt% may record robust results, providing that no deep burial dolomitization has occurred (*36*). Fe speciation is, however, best deployed in addition to other proxies for water column redox conditions (*38*), and, therefore, we use such a strategy by undertaking analysis of redox-sensitive trace elements and I/(Ca + Mg) ratios to more accurately constrain redox conditions on the Siberian Platform.

Redox-sensitive trace element concentrations may be used to provide further constraints on redox conditions in modern and ancient settings (*40*, *85*, *89*, *90*). Of particular note are the behaviors of U, Mo, and Re. Under oxic conditions, Mo and U behave conservatively and occur primarily as MoO^{2-}_4 and $UO_2(CO_3)^{4-}_3$, with oxidation states Mo(VI) and U(VI) (*85*). Under reducing conditions, U(VI) is reduced to insoluble U(IV), resulting in enrichments in the sedimentary record (*91*). Mo may be moderately enriched under reducing conditions but becomes significantly enriched in the presence of free sulfide and is "activated" at a critical HS^- activity to form thiomolybdates ($MoO_xS^{2-}_{4-x}$) (*92*). Mo concentrations may also be enriched by the function of a Mn-Fe particulate shuttle, whereby Mn-Fe (oxyhydr)oxides adsorb molybdate oxyanions, transporting them to the sediment-water interface (*82*). Calibration in modern and ancient settings means that enrichments in Mo and U can be used to assess the redox state of the depositional environment and whether a particulate shuttle is active (*40*). In oxic settings, Re is present as soluble Re(VII) and is reduced to insoluble Re(IV) under dysoxic conditions (*90*). Re enrichment is considered to be a reliable indicator of dysoxic conditions due to accumulation in the sediment at O_2 penetration depths of < ~1 cm (*42*).

I/(Ca + Mg) ratios in carbonates are commonly used to assess redox conditions due to the sensitivity of I to redox conditions in seawater (*45*, *93*). The technique exploits the incorporation of oxidized iodate (IO_3^-) into the calcite and dolomite crystal lattice in place of the carbonate (CO_3^{2-}) ion. It has been shown experimentally that reduced iodide (I^-) does not similarly substitute for the carbonate ion, and, thus, iodine concentrations may be used to assess redox conditions (*45*). Iodine has a high oxidation potential, similar to Mn, and is therefore sensitive to intermediate oxygen concentrations (*45*, *94*). The proxy has been calibrated in a variety of modern and ancient settings and is thus able to assess ancient redox conditions (*45*, *94*–*98*). Some studies suggest that I/(Ca + Mg) ratios may be used as proxies for absolute oxygen concentrations and that I/(Ca + Mg) values <2.5 to 3 μmol/mol in modern foraminiferal samples indicate formation under dysoxic conditions (*44*–*46*); however, defining absolute concentrations is complicated. Low I/(Ca + Mg) values have been reported in the presence of oxic waters due to the slow kinetics of iodide oxidation (*94*), and diagenesis has been shown to reduce I/(Ca + Mg) values (*96*, *99*).

Should a sample set be altered by meteoric diagenesis, sediment- or fluid-buffered diagenesis, and dolomitization, it is possible that I/(Ca + Mg) values may be lowered by as much as ~1.5 to 100% (*99*). Hence, I/(Ca + Mg) values must be carefully considered and a multiproxy approach to corroborate the interpretation of values is preferable. We find no evidence for meteoric diagenesis or dolomitization in our sample set, and published $\delta^{13}C_{carb}$ values are robust and record globally correlatable trends. Given the close relationship of trends in the published $\delta^{13}C_{carb}$ data and our new I/(Ca + Mg) values, it is highly likely that the I/(Ca + Mg) values are recording genuine changes in oxygen concentration. Furthermore, the use of a multiproxy approach has allowed us to cross-reference I/(Ca + Mg) values with other proxy data, such as redox-sensitive trace metal EFs, which yield consistent results. Notwithstanding possible diagenetic effects, major increases and decreases in I/(Ca + Mg) values are, however, robust indicators of elevated and depleted oxygen concentrations in seawater. Here, we interpret our data as such. We do not include the commonly reported sub-oxic-dysoxic threshold of 0.5 μmol/mol and instead refer to values between 0 and 2.6 as "dysoxic" (i.e., with limited oxygen availability).

Supplementary Materials

This PDF file includes:

Supplementary Text
Figs. S1 to S6
Tables S1 to S7
References

REFERENCES AND NOTES

1. D. H. Erwin, M. Laflamme, S. M. Tweedt, E. A. Sperling, D. Pisani, K. J. Peterson, The Cambrian conundrum: Early divergence and later ecological success in the early history of animals. *Science* **334**, 1091–1097 (2011).
2. J. R. Nursall, Oxygen as a prerequisite to the origin of the Metazoa. *Nature* **183**, 1170–1172 (1959).
3. E. A. Sperling, T. H. Boag, M. I. Duncan, C. R. Endriga, J. A. Marquez, D. B. Mills, P. M. Monarrez, J. A. Sclafani, R. G. Stockey, J. L. Payne, Breathless through time: Oxygen and animals across Earth's history. *Biol. Bull.* **243**, 184–206 (2022).
4. R. G. Stockey, D. B. Cole, U. C. Farrell, H. Agić, T. H. Boag, J. J. Brocks, D. E. Canfield, M. Cheng, P. W. Crockford, H. Cui, T. W. Dahl, L. Del Mouro, K. Dewing, S. Q. Dornbos, J. F. Emmings, R. R. Gaines, T. M. Gibson, B. C. Gill, G. J. Gilleaudeau, K. Goldberg, R. Guilbaud, G. Halverson, E. U. Hammarlund, K. Hantsoo, M. A. Henderson, C. M. Henderson, M. S. W. Hodgskiss, A. J. M. Jarrett, D. T. Johnston, P. Kabanov, J. Kimmig, A. H. Knoll, M. Kunzmann, M. A. LeRoy, C. Li, D. K. Loydell, F. A. Macdonald, J. M. Magnall, N. T. Mills, L. M. Och, B. O'Connell, A. Pagès, S. E. Peters, S. M. Porter, S. W. Poulton, S. R. Ritzer, A. D. Rooney, S. Schoepfer, E. F. Smith, J. V. Strauss, G. J. Uhlein, T. White, R. A. Wood, C. R. Woltz, I. Yurchenko, N. J. Planavsky, E. A. Sperling, Sustained increases in atmospheric oxygen and marine productivity in the Neoproterozoic and Palaeozoic eras. *Nat. Geosci.* **17**, 667–674 (2024).
5. B. J. W. Mills, A. J. Krause, I. Jarvis, B. D. Cramer, Evolution of atmospheric O2 through the Phanerozoic, revisited. *Annu. Rev. Earth Planet. Sci.* **51**, 253–276 (2023).
6. E. U. Hammarlund, R. R. Gaines, M. G. Prokopenko, C. Qi, X.-G. Hou, D. E. Canfield, Early Cambrian oxygen minimum zone-like conditions at Chengjiang. *Earth Planet. Sci. Lett.* **475**, 160–168 (2017).
7. R. Guilbaud, B. J. Slater, S. W. Poulton, T. H. P. Harvey, J. J. Brocks, B. J. Nettersheim, N. J. Butterfield, Oxygen minimum zones in the early Cambrian ocean. *Geochem. Perspect. Lett.* **6**, 33–38 (2018).
8. S. K. Sahoo, N. J. Planavsky, G. Jiang, B. Kendall, J. D. Owens, X. Wang, X. Shi, A. D. Anbar, T. W. Lyons, Oceanic oxygenation events in the anoxic Ediacaran ocean. *Geobiology* **14**, 457–468 (2016).

9. G.-Y. Wei, N. J. Planavsky, L. G. Tarhan, X. Chen, W. Wei, D. Li, H.-F. Ling, Marine redox fluctuation as a potential trigger for the Cambrian explosion. *Geology* **46**, 587–590 (2018).
10. G.-Y. Wei, N. J. Planavsky, L. G. Tarhan, T. He, D. Wang, G. A. Shields, W. Wei, H.-F. Ling, Highly dynamic marine redox state through the Cambrian explosion highlighted by authigenic δ238U records. *Earth Planet. Sci. Lett.* **544**, 116361 (2020).
11. T. W. Dahl, J. N. Connelly, D. Li, A. Kouchinsky, B. C. Gill, S. Porter, A. C. Maloof, M. Bizzarro, Atmosphere–ocean oxygen and productivity dynamics during early animal radiations. *Proc. Natl. Acad. Sci. U.S.A.* **116**, 19352–19361 (2019).
12. F. T. Bowyer, R. A. Wood, M. Yilales, Sea level controls on Ediacaran-Cambrian animal radiations. *Sci. Adv.* **10**, eado6462 (2024).
13. T. He, M. Zhu, B. J. W. Mills, P. M. Wynn, A. Y. Zhuravlev, R. Tostevin, P. A. E. P. von Strandmann, A. Yang, S. W. Poulton, G. A. Shields, Possible links between extreme oxygen perturbations and the Cambrian radiation of animals. *Nat. Geosci.* **12**, 468–474 (2019).
14. A. Y. Zhuravlev, E. G. Mitchell, F. Bowyer, R. Wood, A. M. Penny, Increases in reef size, habitat and metacommunity complexity associated with Cambrian radiation oxygenation pulses. *Nat. Commun.* **13**, 7523 (2022).
15. E. A. Sperling, C. A. Frieder, A. V. Raman, P. R. Girguis, L. A. Levin, A. H. Knoll, Oxygen, ecology, and the Cambrian radiation of animals. *Proc. Natl. Acad. Sci. U.S.A.* **110**, 13446–13451 (2013).
16. A. T. Cribb, C. G. Kenchington, B. Koester, B. M. Gibson, T. H. Boag, R. A. Racicot, H. Mocke, M. Laflamme, S. A. F. Darroch, Increase in metazoan ecosystem engineering prior to the Ediacaran-Cambrian boundary in the Nama Group Namibia. *R. Soc. Open Sci.* **6**, 190548 (2019).
17. R. Wood, A. Y. Zhuravlev, Escalation and ecological selectively of mineralogy in the Cambrian radiation of skeletons. *Earth Sci. Rev.* **115**, 249–261 (2012).
18. R. Wood, D. H. Erwin, Innovation not recovery: Dynamic redox promotes metazoan radiations. *Biol. Rev.* **93**, 863–873 (2018).
19. A. Y. Zhuravlev, R. A. Wood, F. T. Bowyer, Cambrian radiation speciation events driven by sea level and redoxcline changes on the Siberian craton. *Sci. Adv.* **9**, eadh2558 (2023).
20. A. Y. Zhuravlev, R. Wood, Dynamic and synchronous changes in metazoan body size during the Cambrian explosion. *Sci. Rep.* **10**, 6784 (2020).
21. T. W. Dahl, M.-L. Siggaard-Andersen, N. H. Schovsbo, D. O. Persson, S. Husted, I. W. Hougård, A. J. Dickson, K. Kjær, A. T. Nielsen, Brief oxygenation events in locally anoxic oceans during the Cambrian solves the animal breathing paradox. *Sci. Rep.* **9**, 11669 (2019).
22. R. A. Wood, S. W. Poulton, A. R. Prave, K.-H. Hoffmann, M. O. Clarkson, R. Guilbaud, J. W. Lyne, R. Tostevin, F. Bowyer, A. M. Penny, A. Curtis, S. A. Kasemann, Dynamic redox conditions control late Ediacaran metazoan ecosystems in the Nama Group Namibia. *Precambrian Res.* **261**, 252–271 (2015).
23. D. H. Erwin, Developmental capacity and the early evolution of animals. *J. Geol. Soc. London* **178**, jgs2020-245 (2021).
24. P. C. J. Donoghue, Z. Yang, The evolution of methods for establishing evolutionary timescales. *Philos. Trans. R. Soc. B: Biol. Sci.* **371**, 20160020 (2016).
25. D. H. Erwin, The origin of animal body plans: A view from fossil evidence and the regulatory genome. *Development* **147**, dev182899 (2020).
26. J. R. Paterson, G. D. Edgecombe, M. S. Y. Lee, Trilobite evolutionary rates constrain the duration of the Cambrian explosion. *Proc. Natl. Acad. Sci. U.S.A.* **116**, 4394–4399 (2019).
27. F. T. Bowyer, A. Y. Zhuravlev, R. Wood, F. Zhao, S. S. Sukhov, R. D. Alexander, S. W. Poulton, M. Zhu, Implications of an integrated late Ediacaran to early Cambrian stratigraphy of the Siberian platform Russia. *Geol. Soc. Am. Bull.* **135**, 2428–2450 (2023).
28. S. S. Sukhov, T. V. Pegel, Yu. Ya. Shabanov, *Regional Stratigraphic Chart of the Cambrian Strata of the Siberian Platform: Decisions of the All-Russian Stratigraphic Meeting on the Development of Stratigraphic Charts of the Upper Precambrian and Palaeozoic of Siberia*. (Novosibirsk, Siberian Scientific-Research Institute of Geology, Geophysics and Mineral Resources, 2021).
29. V. V. Khomentovsky, L. N. Repina, *The Lower Cambrian of the Stratotype Section of Siberia*. (Nauka, 1965).
30. L. N. Repina, Z. V. Borodaevskaya, V. V. Ermak, in *Cambrian of Siberia and Middle Asia* (eds I. T. Zhuravleva, L. N. Repina). *Trans. Inst. Geol. Geophys. Siberian Branch USSR Acad. Sci.* **720**, 3–31 [in Russian] (Moscow, Nauka, 1988).
31. T. V. Pegel, Evolution of Trilobite biofacies in Cambrian basins of the Siberian Platform. *J. Paleo.* **74**, 1000–1019 (2000).
32. E. Bushuev, I. Goryaeva, V. Pereladov, New discoveries of the oldest trilobites Profallotaspis and Nevadella in the northeastern Siberian Platform Russia. *Bull. Geosci.* **89**, 347–364 (2014).
33. E. Landing, M. D. Schmitz, G. Geyer, R. B. Trayler, S. A. Bowring, Precise early Cambrian U–Pb zircon dates bracket the oldest trilobites and archaeocyaths in Moroccan West Gondwana. *Geol. Mag.* **158**, 219–238 (2021).
34. S. S. Sukhov, Yu. Ya. Shabanov, T. V. Pegel, S. V. Saraev, Y. F. Filippov, I. V. Korovnikov, V. M. Sundukov, A. B. Fedorov, A. I. Varlamov, A. S. Efimov, V. A. Kontorovich, A. E. Kontorovich, *Stratigraphy of Oil and Gas Basins of Siberia. Cambrian of Siberian Platform, V. 1: Stratigraphy.* (Novosibirsk, Institute of Petroleum Geology and Geophysics, Siberian Branch, Russian Academy of Sciences, Novosibirsk, 2016).
35. M. D. Brasier, A. Y. Rozanov, A. Y. Zhuravlev, R. M. Corfield, L. A. Derry, A carbon isotope reference scale for the Lower Cambrian succession in Siberia: Report of IGCP Project 303. *Geol. Mag.* **131**, 767–783 (1994).
36. M. O. Clarkson, S. W. Poulton, R. Guilbaud, R. A. Wood, Assessing the utility of Fe/Al and Fe-speciation to record water column redox conditions in carbonate-rich sediments. *Chem. Geol.* **382**, 111–122 (2014).
37. S. W. Poulton, D. E. Canfield, Ferruginous conditions: A dominant feature of the ocean through Earth's history. *Elements* **7**, 107–112 (2011).
38. S. W. Poulton, *The Iron Speciation Paleoredox Proxy. Elements in Geochemical Tracers in Earth System Science*, (Cambridge Univ. Press, 2021).
39. C. Krewer, S. W. Poulton, R. J. Newton, C. März, B. J. W. Mills, T. Wagner, Controls on the termination of cretaceous oceanic anoxic event 2 in the Tarfaya Basin, Morocco. *Am. J. Sci.* **324**, 11 (2024).
40. N. Tribovillard, T. J. Algeo, F. Baudin, A. Riboulleau, Analysis of marine environmental conditions based onmolybdenum–uranium covariation—Applications to Mesozoic paleoceanography. *Chem. Geol.* **324-325**, 46–58 (2012).
41. D. B. Cole, D. B. Mills, D. H. Erwin, E. A. Sperling, S. M. Porter, C. T. Reinhard, N. J. Planavsky, On the co-evolution of surface oxygen levels and animals. *Geobiology* **18**, 260–281 (2020).
42. J. L. Morford, S. R. Emerson, E. J. Breckel, S. H. Kim, Diagenesis of oxyanions (V, U, Re, and Mo) in pore waters and sediments from a continental margin. *Geochim. Cosmochim. Acta* **69**, 5021–5032 (2005).
43. N. Glock, V. Liebetrau, A. Eisenhauer, I/Ca ratios in benthic foraminifera from the Peruvian oxygen minimum zone: Analytical methodology and evaluation as a proxy for redox conditions. *Biogeosciences* **11**, 7077–7095 (2014).
44. Z. Lu, B. A. A. Hoogakker, C.-D. Hillenbrand, X. Zhou, E. Thomas, K. M. Gutchess, W. Lu, L. Jones, R. E. M. Rickaby, Oxygen depletion recorded in upper waters of the glacial Southern Ocean. *Nat. Commun.* **7**, 11146 (2016).
45. Z. Lu, H. C. Jenkyns, R. E. M. Rickaby, Iodine to calcium ratios in marine carbonate as a paleo-redox proxy during oceanic anoxic events. *Geology* **38**, 1107–1110 (2010).
46. K. Huang, M. Cheng, T. J. Algeo, J. Hu, H. Wang, Z. Zhang, M. S. Dodd, Y. Wu, W. Guo, C. Li, Interaction of Shibantan Biota and environment in the terminal Ediacaran ocean: Evidence from I/(Ca+Mg) and sulfur isotopes. *Precambrian Res.* **379**, 106814 (2022).
47. A. S. Merdith, S. E. Williams, A. S. Collins, M. G. Tetley, J. A. Mulder, M. L. Blades, A. Young, S. E. Armistead, J. Cannon, S. Zahirovic, R. D. Müller, Extending full-plate tectonic models into deep time: Linking the Neoproterozoic and the Phanerozoic. *Earth Sci. Rev.* **214**, 103477 (2021).
48. T. W. Wong Hearing, A. Pohl, M. Williams, Y. Donnadieu, T. H. P. Harvey, C. R. Scotese, P. Sepulchre, A. Franc, T. R. A. Vandenbroucke, Quantitative comparison of geological data and model simulations constrains early Cambrian geography and climate. *Nat. Commun.* **12**, 3868 (2021).
49. V. A. Atashkin, T. V. Pegel, L. N. Repina, A. Y. Rozanov, Y. Y. Shabanov, A. Y. Zhuravlev, S. S. Sukhov, V. M. Sundukov, The Cambrian system on the Siberian platform: Correlation chart and explanatory notes. *Internat. Un. Geol. Sci. Publ.* **27**, 1–133 (1991).
50. T. H. Torsvik, L. R. M. Cocks, Gondwana from top to base in space and time. *Gondw. Res.* **24**, 999–1030 (2013).
51. G. W. O'Brien, A. R. Milnes, H. H. Veeh, D. T. Heggie, S. R. Riggs, D. J. Cullen, J. F. Marshall, P. J. Cook, Sedimentation dynamics and redox iron-cycling: Controlling factors for the apatite—Glauconite association on the East Australian continental margin. *Geol. Soc. Spec. Publ.* **52**, 61–86 (1990).
52. J.-G. Bréhéret, Glauconitization episodes in marginal settings as echoes of mid-Cretaceous anoxic events in the Vocontian basin (SE France). *Geol. Soc. Spec. Publ.* **58**, 415–425 (1991).
53. J. R. Creveling, D. T. Johnston, S. W. Poulton, B. Kotrc, C. März, D. P. Schrag, A. H. Knoll, Phosphorus sources for phosphatic Cambrian carbonates. *GSA Bull.* **126**, 145–163 (2014).
54. K. B. Föllmi, Sedimentary condensation. *Earth Sci. Rev.* **152**, 143–180 (2016).
55. R. L. Freeman, B. F. Dattilo, C. E. Brett, An integrated stratinomic model for the genesis and concentration of "small shelly fossil"-style phosphatic microsteinkerns in not-so-exceptional conditions. *Palaeogeogr. Palaeoclimatol. Palaeoecol.* **535**, 109344 (2019).
56. S. B. Pruss, B. C. Gill, Life on the edge: The Cambrian marine realm and oxygenation. *Annu. Rev. Earth Planet. Sci.* **52**, 109–132 (2024).
57. S. E. Peters, R. R. Gaines, Formation of the 'Great Unconformity' as a trigger for the Cambrian explosion. *Nature* **484**, 363–366 (2012).
58. V. A. Luchinina, I. V. Korovnikov, N. V. Novozhilova, D. A. Tokarev, Benthic Cambrian biofacies of the Siberian Platform (hyoliths, small shelly fossils, archeocyaths, trilobites and calcareous algae). *Stratigr. Geol. Correl.* **21**, 131–149 (2013).
59. A. Y. Zhuravlev, R. A. Wood, The two phases of the Cambrian explosion. *Sci. Rep.* **8**, 16656 (2018).

60. E. A. Sperling, A. H. Knoll, P. R. Girguis, The ecological physiology of Earth's second oxygen revolution. *Ann. Rev. Ecol. Evol. Syst.* **46**, 215–235 (2015).
61. M. J. Pushie, B. R. Pratt, T. C. MacDonald, G. N. George, I. J. Pickering, Evidence for biogenic copper (hemocyanin) in the middle Cambrian arthropod Marrella from the Burgess Shale. *PALAIOS* **29**, 512–524 (2014).
62. J.-B. Hou, N. C. Hughes, M. J. Hopkins, The trilobite upper limb branch is a well-developed gill. *Sci. Adv.* **7**, eabe7377 (2021).
63. J. B. Graham, Ecological, evolutionary, and physical factors influencing aquatic animal respiration. *Am. Zool.* **30**, 137–146 (1990).
64. H. B. Whittington,, B. D. E. Chatterton, S. E. Speyer, R. A. Fortey, R. M. Owens, W. T. Chang, W. T. Dean, P. A. Jell, J. R. Laurie, A. R. Palmer, L. N. Repina, A. W. A. Rushton, J. H. Shergold, E. N. K. Clarkson, N. V. Wilmot, S. R. A. Kelly, Part O, revised. Trilobita (Introduction, Order Agnostida, Order Redlichiida) *Treatise on Invertebrate Paleontology* (Geological Society of America and University of Kansas, 1997), p. 530.
65. D. B. Mills, L. M. Ward, C. Jones, B. Sweeten, M. Forth, A. H. Treusch, D. E. Canfield, Oxygen requirements of the earliest animals. *Proc. Natl. Acad. Sci. U.S.A.* **111**, 4168–4172 (2014).
66. V. Micaroni, F. Strano, R. McAllen, L. Woods, J. Turner, L. Harman, J. J. Bell, Adaptive strategies of sponges to deoxygenated oceans. *Glob. Change Biol.* **28**, 1972–1989 (2022).
67. J. V. Bannister, The respiration in air and in water of the limpets *Patella caerulea* (L.) and *Patella lusitanica* (Gmelin). *Comp. Biochem. Physical.* **49**, 407–411 (1974).
68. S. Calderon Lievanos, "Respuesta Bioenergética, Actividad Bioquímica Y Expresión Proteómica A Corto Y Largo Plazo, En Abulón Azul (*Haliotis Fulgens*, Philippi 1845) Expuesto A Cambios Repentinos De Estrés Térmico Y De Hipoxia," thesis, Centro de Investigaciones Biológicas del Noroeste, S.C. (2019).
69. H. Szaniawski, New evidence for the protoconodont origin of chaetognaths. *Acta Palaeontol. Pol.* **47**, 405–419 (2002).
70. D. Shu, S. Conway Morris, J. Han, J. F. Hoyal Cuthill, Z. Zhang, M. Cheng, H. Huang, Multi-jawed chaetognaths from the Chengjiang Lagerstätte (Cambrian, series 2, stage 3) of Yunnan, China. *Palaeontology* **60**, 763–772 (2017).
71. D. Pauly, C. Liang, W. Xian, E. Chu, N. Bailly, The sizes, growth and reproduction of arrow worms (Chaetognatha) in light of the gill-oxygen limitation theory (GOLT). *J. Mar. Sci. Eng.* **9**, 1397 (2021).
72. A. K. Val'kov, Biostratigraphy of the Lower Cambrian in the East of the Siberian Platform (Uchur-Maya Region). (Nauka, 1982).
73. A. K. Val'kov, Biostratigraphy of the Lower Cambrian in the East of the Siberian Platform (Yudoma-Olenek Region). (Nauka, 1987).
74. A. Kouchinsky, S. Bengtson, W. Feng, R. Kutygin, A. Val'kov, The lower cambrian fossil anabaritids: Affinities, occurrences and systematics. *J. Syst. Palaeontol.* **7**, 241–298 (2009).
75. A. Kouchinsky, R. Alexander, S. Bengtson, F. Bowyer, S. Clausen, L. E. Holmer, K. A. Kolesnikov, I. V. Korovnikov, V. E. Pavlov, C. B. Skovsted, G. Ushatinskaya, R. Wood, A. Y. Zhuravlev, Early–Middle Cambrian stratigraphy and faunas from northern Siberia. *Acta Palaeontol. Pol.* **67**, 341–464 (2022).
76. P. M. Novack-Gottshall, Ecosystem-wide body-size trends in Cambrian–Devonian marine invertebrate lineages. *Paleobiology* **34**, 210–228 (2008).
77. J. L. Payne, A. G. Boyer, J. H. Brown, S. Finnegan, M. Kowalewski, R. A. Krause Jr., S. K. Lyons, C. R. McClain, D. W. McShea, P. M. Novack-Gottshall, F. A. Smith, J. A. Stempien, S. C. Wang, Two-phase increase in the maximum size of life over 3.5 billion years reflects biological innovation and environmental opportunity. *Proc. Natl. Acad. Sci. U.S.A.* **106**, 24–27 (2009).
78. F. T. Bowyer, A. Y. Zhuravlev, R. Wood, G. A. Shields, Y. Zhou, A. Curtis, S. W. Poulton, D. J. Condon, C. Yang, M. Zhu, Calibrating the temporal and spatial dynamics of the Ediacaran - Cambrian radiation of animals. *Earth Sci. Rev.* **225**, 103913 (2022).
79. S. W. Poulton, D. E. Canfield, Development of a sequential extraction procedure for iron: Implications for iron partitioning in continentally derived particulates. *Chem. Geol.* **214**, 209–221 (2005).
80. L. J. Alcott, A. J. Krause, E. U. Hammarlund, C. J. Bjerrum, F. Scholz, Y. Xiong, A. J. Hobson, L. Neve, B. J. W. Mills, C. März, B. Schnetger, A. Bekker, S. W. Poulton, Development of iron speciation reference materials for Palaeoredox analysis. *Geostand. Geoanal. Res.* **44**, 581–591 (2020).
81. T. He, R. J. Newton, P. B. Wignall, S. Reid, J. Dal Corso, S. Takahashi, H. Wu, S. Todaro, P. Di Stefano, V. Randazzo, M. Rigo, A. M. Dunhill, Shallow ocean oxygen decline during the end-Triassic mass extinction. *Glob. Planet. Change* **210**, 103770 (2022).
82. T. J. Algeo, N. Tribovillard, Environmental analysis of paleoceanographic systems based on molybdenum–Uranium covariation. *Chem. Geol.* **268**, 211–225 (2009).
83. R. M. Gaschnig, R. L. Rudnick, W. F. McDonough, A. J. Kaufman, J. W. Valley, Z. Hu, S. Gao, M. L. Beck, Compositional evolution of the upper continental crust through time, as constrained by ancient glacial diamictites. *Geochim. Cosmochim. Acta* **186**, 316–343 (2016).
84. K. Hans Wedepohl, The composition of the continental crust. *Geochim. Cosmochim. Acta* **59**, 1217–1232 (1995).
85. N. Tribovillard, T. J. Algeo, T. Lyons, A. Riboulleau, Trace metals as paleoredox and paleoproductivity proxies: An update. *Chem. Geol.* **232**, 12–32 (2006).
86. R. Raiswell, D. S. Hardisty, T. W. Lyons, D. E. Canfield, J. D. Owens, N. J. Planavsky, S. W. Poulton, C. T. Reinhard, The iron paleoredox proxies: A guide to the pitfalls, problems and proper practice. *Am. J. Sci.* **318**, 491–526 (2018).
87. S. W. Poulton, R. Raiswell, The low-temperature geochemical cycle of iron: From continental fluxes to marine sediment deposition. *Am. J. Sci.* **302**, 774–805 (2002).
88. S. W. Poulton, M. D. Krom, R. Raiswell, A revised scheme for the reactivity of iron (oxyhydr)oxide minerals towards dissolved sulfide. *Geochim. Cosmochim. Acta* **68**, 3703–3715 (2004).
89. S. E. Calvert, T. F. Pedersen, Geochemistry of recent oxic and anoxic marine sediments: Implications for the geological record. *Mar. Geol.* **113**, 67–88 (1993).
90. J. Crusius, S. Calvert, T. Pedersen, D. Sage, Rhenium and molybdenum enrichments in sediments as indicators of oxic, suboxic and sulfidic conditions of deposition. *Earth Planet. Sci. Lett.* **145**, 65–78 (1996).
91. R. F. Anderson, M. Q. Fleisher, A. P. LeHuray, Concentration, oxidation state, and particulate flux of uranium in the Black Sea. *Geochim. Cosmochim. Acta* **53**, 2215–2224 (1989).
92. G. R. Helz, C. V. Miller, J. M. Charnock, J. F. W. Mosselmans, R. A. D. Pattrick, C. D. Garner, D. J. Vaughan, Mechanism of molybdenum removal from the sea and its concentration in black shales: EXAFS evidence. *Geochim. Cosmochim. Acta* **60**, 3631–3642 (1996).
93. G. T. F. Wong, P. G. Brewer, The marine chemistry of iodine in anoxic basins. *Geochim. Cosmochim. Acta* **41**, 151–159 (1977).
94. W. Lu, A. J. Dickson, E. Thomas, R. E. M. Rickaby, P. Chapman, Z. Lu, Refining the planktic foraminiferal I/Ca proxy: Results from the Southeast Atlantic Ocean. *Geochim. Cosmochim. Acta* **287**, 318–327 (2020).
95. D. S. Hardisty, Z. Lu, N. J. Planavsky, A. Bekker, P. Philippot, X. Zhou, T. W. Lyons, An iodine record of Paleoproterozoic surface ocean oxygenation. *Geology* **42**, 619–622 (2014).
96. D. S. Hardisty, Z. Lu, A. Bekker, C. W. Diamond, B. C. Gill, G. Jiang, L. C. Kah, A. H. Knoll, S. J. Loyd, M. R. Osburn, N. J. Planavsky, C. Wang, X. Zhou, T. W. Lyons, Perspectives on Proterozoic surface ocean redox from iodine contents in ancient and recent carbonate. *Earth Planet. Sci. Lett.* **463**, 159–170 (2017).
97. W. Lu, S. Wörndle, G. P. Halverson, X. Zhou, A. Bekker, R. H. Rainbird, D. S. Hardisty, T. W. Lyons, Z. Lu, Iodine proxy evidence for increased ocean oxygenation during the Bitter Springs Anomaly. *Geochem. Persp. Let.* **53–57**, 53–57 (2017).
98. R. He, A. Pohl, A. Prow, G. Jiang, C. C. Huan, M. R. Saltzman, Z. Lu, The dynamic ocean redox evolution during the late Cambrian SPICE: Evidence from the I/Ca proxy. *Global Planet. Change* **233**, 104354 (2024).
99. K. V. Lau, D. S. Hardisty, Modeling the impacts of diagenesis on carbonate paleoredox proxies. *Geochim. Cosmochim. Acta* **337**, 123–139 (2022).
100. M. Zhu, A. Y. Zhuravlev, R. A. Wood, F. Zhao, S. S. Sukhov, A deep root for the Cambrian explosion: Implications of new bio- and chemostratigraphy from the Siberian Platform. *Geology* **45**, 459–462 (2017).
101. Yu. L. Pel'man, N. A. Aksarina, S. P. Koneva, L. E. Popov, L. P. Sobolev, G. T. Ushatinskaya, *The oldest brachiopods from the territory of northern Eurasia*, (Novosibirsk, OIGGiM SO RAN., 1992), p. 145 [in Russian].
102. V. A. Datsenko, L. T. Zhuravleva, N. P. Lazarenko, Yu. N. Popov, N. E. Chernysheva, Biostratigraphy and fauna of the Cambrian deposits of the northwestern Siberian Platform. (Nauchno-Issledovatel'skiy Institut Geologii Arktiki, Trudy 155, 1968), pp. 1–213 [in Russian].
103. V. V. Khomentovsky, G. A. Karlova, in *Late Precambrian and Early Palaeozoic of Siberia. Actual Problems of the Stratigraphy* (eds V. V. Khomentovsky, Yu. K. Sovetov) 23–61 [in Russian] (Institute of Geology and Geophysics, Siberian Branch, USSR Academy of Sciences, 1989).
104. V. V. Khomentovsky, G. A. Karlova, in *Late Precambrian and Early Palaeozoic of Siberia. Siberian Platform and Its Borderland* [in Russian], V. V. Khomentovsky (United Institute of Geology, Geophysics and Mineralogy, Siberian Branch, USSR Academy of Sciences, 1991), p. 3–44.
105. K. E. Nagovitsin, V. I. Rogov, V. V. Marusin, G. A. Karlova, A. V. Kolesnikov, N. V. Bykova, D. V. Grazhdankin, Revised Neoproterozoic and Terreneuvian stratigraphy of the Lena-Anabar Basin and north-western slope of the Olenek Uplift, Siberian Platform. *Precambrian Res.* **270**, 226–245 (2015).
106. A. Kouchinsky, S. Bengtson, E. Landing, M. Steiner, M. Vendrasco, K. Ziegler, Terreneuvian stratigraphy and faunas from the Anabar Uplift, Siberia. *Acta Palaeontol. Pol.* **62**, 311–440 (2017).
107. A. K. Valkov, *Biostratigraphy and Hyoliths of the Cambrian of Northeastern Siberian Platform*, (Moscow, Nauka, 1975), p. 139.
108. V. V. Khomentovsky, A. B. Fedorov, G. A. Karlova, Lower Cambrian boundary in the inner areas on the North Siberian Platform. *Stratigr. Geol. Correl.* **6**, 3–9 (1998).
109. A. Yu. Rozanov, V. V. Missarzhevsky, N. A. Volkova, L. G. Voronova, I. N. Krylov, B. M. Keller, I. K. Korolyuk, K. Lendzion, R. Michniak, N. G. Pykhova, A. D. Sidorov, *The Tommotian Stage and the Cambrian Lower Boundary Problem* (English translation, Amerind Publishing Co., 1981; Nauka, 1969).

110. S. M. Rowland, V. A. Luchinina, I. V. Korovnikov, D. P. Sipin, A. I. Tarletskov, A. V. Fedoseev, Biostratigraphy of the Vendian-Cambrian Sukharikha River section, northwestern Siberian Platform. *Can. J. Earth Sci.* **35**, 339–352 (1998).
111. V. V. Khomentovsky, G. A. Karlova, The boundary between Nemakit-Daldynian and Tommotian stages (Vendian-Cambrian Systems) of Siberia. *Stratigr. Geol. Correl.* **10**, 13–34 (2002).
112. A. I. Varlamov, A. Yu. Rozanov, V. V. Khomentovsky, Yu. Ya. Shabanov, G. P. Abaimova, Yu. E. Demidenko, G. A. Karlova, I. V. Korovnikov, V. A. Luchinina, Ya. E. Malakhovskaya, P. Yu. Parkhaev, T. V. Pegel, N. A. Skorlotova, V. M. Sundukov, S. S. Sukhov, A. B. Fedorov, L. K. Kipriyanova, *The Cambrian System of the Siberian Platform. Part 1: The Aldan-Lena Region*. (Moscow; Novosibirsk, PIN RAS. 2008) p. 300.
113. V. V. Khomentovsky, G. A. Karlova, The boundary between Nemakit-Daldynian and Tommotian stages (Vendian-Cambrian) of Siberia. *Stratigr. Geol. Correl.* **10**, 217–238 (2002).
114. V. I. Korshunov, L. N. Repina, V. A. Sysoev, To the structure of the Pestrotsvet Formation on the East of the Aldan Anteclise. (*Geol. Geofiz*., 10, 1969), pp. 18–21 [in Russian].
115. A. K. Val'kov, Distribution of the oldest skeletal organisms and correlation of the Cambrian lower boundary in southeastern part of the Siberian Platform in *Late Precambrian and Early Palaeozoic of Siberia. Vendian Strata*, V. V. Khomentovsky, ed. (United Institute of Geology, Geophysics and Mineralogy, Siberian Branch, USSR Academy of Sciences, Novosibirsk, 1983), pp. 37–48. [in Russian].
116. A. Yu. Rozanov, P. Yu. Parkhaev, Yu. E. Demidenko, G. A. Karlova, I. V. Korovnikov, Yu. Ya. Shabanov, A. Yu. Ivantsov, V. A. Luchinina, Ya. E. Malakhovskaya, L. M. Melnikova, E. B. Naimark, A. G. Ponomarenko, N. A. Skorlotova, V. M. Sundukov, D. A. Tokarev, G. T. Ushatinskaya, L. K. Kipriyanova, *Fossils from the Lower Cambrian Stage Stratotypes*, (Moscow, PIN RAN., 2010), p. 228 [in Russian].
117. L. Devaere, S. Clausen, M. Steiner, J.-J. Álvaro, D. Vachard, Chronostratigraphic and palaeogeographic significance of an early Cambrian microfauna from the Heraultia Limestone, northern Montagne Noire, France. *Palaeontol. Electronica* **16**, 91 (2013).
118. P. Y. Parkhaev, Y. E. Demidenko, M. A. Kulsha, The problematic fossil *Mobergella radiolata* as an index species of the Lower Cambrian stages. *Stratigr. Geol. Correl.* **28**, 135–156 (2020).
119. P. Y. Parkhaev, Y. E. Demidenko, Zooproblematica and mollusca from the Lower Cambrian Meishucun section (Yunnan, China) and taxonomy and systematics of the Cambrian small shelly fossils of China. *Paleontol. J.* **44**, 883–1161 (2010).
120. P. Y. Parkhaev, G. A. Karlova, Taxonomic revision and evolution of Cambrian mollusks of the genus *Aldanella* Vostokova, 1962 (Gastropoda: Archaeobranchia). *Paleontol. J.* **45**, 1145–1205 (2011).
121. P. Y. Parkhaev, Two new species of the Cambrian helcionelloid mollusks from the northern part of the Siberian Platform. *Paleontol. J.* **39**, 615–619 (2005).
122. A. P. Gubanov, J. S. Peel, The early Cambrian helcionelloid mollusc *Anabarella* Vostokova. *Palaeontology* **46**, 1073–1087 (2003).
123. V. V. Khomentovsky, G. A. Karlova, On the lower boundary of the Pestrotsvet Formation in the Aldan River basin in *Late Precambrian and Early Palaeozoic of Siberia. Siberian Platform and the Outer Zone of the Altay-Sayan Foldbelt*, V. V. Khomentovsky, ed. (United Institute of Geology, Geophysics and Mineralogy, Siberian Branch, USSR Academy of Sciences, Novosibirsk 1986), pp. 3–22 [in Russian].
124. V. V. Khomentovsky, G. A. Karlova, Specifics of the ecology of Vendian-Cambrian small shelly fossil biota from Siberian Platform. *Stratigr. Geol. Correl.* **2**, 8–17 (1994).
125. G. Geyer, The Moroccan fallotaspidid trilobites revisited. *Ther. Ber.* **18**, 89–199 (1996).
126. G. Geyer, The earliest known West Gondwana trilobites from the Anti-Atlas of Morocco, with a revision of the Family Bigotinidae Hupé, 1953. *Foss. Strata* **64**, 55–153 (2019).
127. L. N. Repina, Evolution of trilobites at the early stages of their historical development. *Trans. Inst. Geol. Geophys. Siberian Branch USSR Acad. Sci.* **764**, 34–44 (1990).
128. L. N. Repina, Dependence of morphologic features on habitat conditions in trilobites and evaluation of their significance for the systematics of the superfamily Olenelloidea in *Environment and Life in the Geological Past (Problems of Ecostratigraphy)*, O. A. Betekhtina, I. T. Zhuravleva, eds. (Novosibirsk, Nauka, 1979), pp. 11–30 [in Russian].
129. N. P. Meshkova, Lower Cambrian hyoliths of the Siberian Platform. *Trans. Inst. Geol. Geophys. Siberian Branch USSR Acad. Sci.* **1**, 110 (1974). .
130. I. N. Krasilova, Fordillids (Bivalvia) from the Lower Cambrian of the Siberian Platform. *Paleontologicheskiy Zhurnal* **1977**, 42–48 (1977).
131. V. A. Astashkin, A. K. Valkov, L. G. Voronova, N. V. Grigorieva, L. I. Egorova, E. A. Zhegallo, A. Yu. Zhuravlev, I. T. Zhuravleva, V. I. Korshunov, V. A. Luchinina, V. V. Missarzhevsky, L. M. Melnikova, N. P. Meshkova, D. V. Osadchaya, Yu. L. Pelman, L. N. Repina, A. Yu. Rozanov, V. M. Sundukov, N. P. Suvorova, V. A. Sysoev, V. D. Fonin, *Early Cambrian Stage Subdivision of Siberia. Atlas of Fossils*. (Institute of Geology and Geophysics, Siberian Branch, USSR Academy of Sciences, Transactions 558. Nauka, Moscow, 1983), p. 216 [in Russian].
132. V. V. Khomentovsky, A. K. Valkov, G. A. Karlova S. V. Nuzhnov, Key section of Precambrian Cambrian deposits of the Gonam River in Late Precambrian and Lower Palaeozoic of Siberia. Vendian Deposits (Novosibirsk, 1983), pp. 29–44.
133. Yu. L. Pel'man, V. V. Ermak, A. B. Fedorov, V. A. Luchinina, I. T. Zhuravleva, L. N. Repina, V. I. Bondarev, Z. V. Borodaevskaya, [New data on the upper Precambrian and lower Cambrian stratigraphy and palaeontology of the r. Dzhanda (right tributary of the r. Aldan)] in Biostratigraphy and Paleontology of the Cambrian of Northern Asia, L. N. Repina, ed. (Institut Geologii i Geofiziki Sibirskogo Otdeleniya Akademii Nauk SSSR, Trudy 765, 1990), pp. 3–43 1990 [in Russian].
134. V. A. Datsenko, I. T. Zhuravleva, N. P. Lazarenko, Yu. N. Popov, N. E. Chernysheva, Biostratigraphy and fauna of the Cambrian deposits of the northwestern Siberian Platform. Trans. Sci.-Res. Inst. Geol. Arctic 155 [in Russian] (Nedra, 1968).
135. I. T. Zhuravleva, Yu. K. Sovetov, T. Titorenko, N. in *Stratigraphy of the Lower Cambrian and Upper Precambrian in the South of the Siberian Platform*, B. S. Sokolov [in Russian] (Nauka, 1969b), pp. 13–16.
136. Z. A. Akul'cheva, E. M. Galperova, E. L. Drobkova, L. A. Lysova, T. N. Titorenko, A. A. Treshchetenkova, Z. Kh. Fayzulina, Mota strata and their analogies in the Irkutsk Amphitheater in *Boundary Strata of the Precambrian and Cambrian of the Siberian Platform (Biostratigraphy, Palaeontology, Conditions of the Formation)*, N. P. Meshkova, I. V. Nikolaeva, eds. (Institut Geologii i Geofiziki Sibirskogo Otdeleniya Akademii Nauk SSSR, Trudy 475 Novosibirsk, Nauka, 1981), pp. 65–139. [in Russian].
137. T. I. Burtseva, I. T. Zhuravleva, First find of archaeocyaths in the Irkutsk Amphitheatre. Dokl. Akad. Nauk SSSR 106, 885–888 [in Russian] (1956).
138. I. N. Dyatlova, A. N. Deonov, V. R. Trofimov in *Biostratigraphy and Palaeontology of the Cambrian of Northern Asia*, L. N. Repina, ed. *Trans. Inst. Geol. Geophys. Siberian Branch USSR Acad. Sci.* 765, Nauka, 1990), pp. 123–135 [in Russian].
139. V. V. Gritsik, in *Problems of Lower Cambrian Palaeontology and Biostratigraphy of Siberia and the Far East*, I. T. Zhuravleva, ed. (Nauka, 1969), pp. 186–202 [in Russian].
140. A. Kouchinsky, S. Bengtson, S. Clausen, M. J. Vendrasco, An early Cambrian fauna of skeletal fossils from the Emyaksin Formation, northern Siberia. *Acta Palaeontol. Pol.* **60**, 421–512 (2015).
141. N. P. Meshkova, I. V. Nikolaeva, Y. P. Kulikov, I. T. Zhuravleva, V. A. Luchinina, D. I. Musatov, S. D. Sidoras, Stratigraphy of Precambrian-Cambrian boundary strata on the North of the Anabar Uplift, (ed. Zhuravleva, I.T., Lower and Middle Cambrian stratigraphy and palaeontology of the U.S.S.R.). Trans. Inst. Geol. Geophys. Siberian Branch USSR Acad. Sci, 296, 3–22 (1976).
142. L. I. Egorova, V. E. Savistkiy, *Stratigraphy and Biofacies of the Cambrian of the Siberian Platform (Western Anabar Area).* (*Trans. Sib. Sci.-Res. Inst. Geol. Geophys. Miner. Res.*) **43** [in Russian] (Nedra, 1969).
143. V. M. Sundukov, F. B. Fedorov, in *Biostratigraphy and Palaeontology of the Cambrian of Northern Asia*, I. T. Zhuravleva, ed. (*Trans. Inst. Geol. Geophys. Siberian Branch USSR Acad. Sci.* 669, Nauka, 1986), pp. 108–119 [in Russian].
144. B. B. Shishkin, Vendian deposits of the southestern part of Siberian Platform. *Geol. Miner. Resour. Sib.* **3**, 3–10 (2011).
145. V. I. Korshunov, *Lower Cambrian Biostratigraphy and Archaeocyaths of the Northeastern Aldan Anteclise* (Yakutsk Publishers, 1972) [in Russian].
146. A. I. Goryachev, M. A. Zharkov, in *Stratigraphy of the Lower Cambrian and Upper Precambrian in the South of the Siberian Platform*, B. S. Sokolov, ed., (Nauka, 1969), pp. 17–33 [in Russian].
147. V. V. Marusin, A. A. Kolesnikova, B. B. Kochnev, N. B. Kuznetsov, B. G. Pokrovsky, T. V. Romanyuk, G. A. Karlova, S. V. Rud'ko, A. V. Shatsillo, A. S. Dubenskiy, V. S. Sheshukov, S. M. Lyapunov, Detrital zircon age and biostratigraphic and chemostratigraphic constraints on the Ediacaran–Cambrian transitional interval in the Cis-Sayans Uplift, southwestern Siberian Platform. *Geol. Mag.* **158**, 1156–1172 (2021).
148. M. A. Zharkov, Yu. K. Sovetov, in *Stratigraphy of the Lower Cambrian and Upper Precambrian in the South of the Siberian Platform*, B. S. Sokolov, ed., (Nauka, 1969), pp. 34–55 [in Russian].
149. V. M. Sundukov, New archaeocyaths from the Lower Cambrian of the Lena and Kotuy. *Paleontol. Zh.* **1983**, 13–17 (1983).
150. I. T. Zhuravleva in *Biostratigraphy and Palaeontology of the Lower and Middle Cambrian of Northern Asia*, N. P. Meshkova, ed. (*Trans. Inst. Geol. Geophys. Siberian Branch USSR Acad. Sci.* 541, Nauka, 1983), pp. 81–94 [in Russian].
151. L. N. Repina, V. A. Luchinina, To the biostratigraphy of the lower part of the Lower Cambrian in northwestern Prinabar'e (R. Fomich) In N. P. Meshkova, I. V. Nikolaeva, eds. (Boundary Strata of the Precambrian and Cambrian of the Siberian Platform (Biostratigraphy, Palaeontology, Conditions of the Formation). Institut Geologii i Geofiziki Sibirskogo Otdeleniya Akademii Nauk SSSR, Trudy 475, 3–19. Novosibirsk, Nauka, 1981 [in Russian].
152. V. E. Savitskiy, New data on the stratigraphy of the Cambrian strata on the Anabar anteclise. *Collective Papers on the Geology of the Arctic* (1959), vol. 102 [in Russian].
153. N. P. Meshkova, I. T. Zhuravleva, V. A. Luchinina, Lower Cambrian and the lower part of the Middle Cambrian of the Olenek Uplift in *Problems of Paleontology and Biostratigraphy of the Lower Cambrian of Siberia and the Far* East, I. T. Zhuravleva, ed., (Novosibirsk, Nauka, 1973), pp. 194–214 [in Russian].

154. V. E. Savitskiy, Yu.Ya. Shabanov, B. B. Shishkin, Stratigraphy of the Precambrian and Cambrian strata of the Igarka area. Sibirskiy Institut Geologii, Geofiziki i Mineral'nogo Syr'ya, Trudy, Seriya Neftyanaya Geologiya Neftegazonosnykh Rayonov Sibiri, 32, Pt II 1964 (in Russian).
155. I. V. Korovnikov, Trilobites of the suborder Eodiscina from the Lower Cambrian of the northeastern Siberian Platform (Khorbosuonka River section). *Paleontol. J.* **41**, 614–620 (2007).
156. L. I. Egorova, L. N. Repina, N. P. Suvorova, Lower Cambrian stage subdivision of the Siberia. Atlas of fossils. Trans. Inst. Geol. *Geophys. Siberian Branch USSR Acad. Sci.* **558**, 1–216 (1983).
157. T. V. Pegel, L. I. Egorova, Yu. Ya. Shabanov, I. V. Korovnikov, V. A. Luchinina, A. K. Salikhova, V. M. Sundukov, A. B. Fedorov, A. Yu. Zhuravlev, P. Yu. Parkhaev, Yu. E. Demidenko, Stratigraphy of Oil and Gas Basins of Siberia. Cambrian of Siberian Platform. V. 2 – Palaeontology [in Russian] (Institute of Petroleum Geology and Geophysics, Siberian Branch, Russian Academy of Sciences, 2016).
158. A. I. Varlamov, L. I. Egorova, Stratigrafiya nizhnekembriyskikh otlozheniy t. Tol'by (yug Sibirskoy platformy) in *Biostratigrafiya i paleontologiya kembriya Severnoy Azii*, I. T. Zhuravleva, ed. (Trudy Akademiya Nauk SSSR, Sibirskoe otdelenie, Nauka, Novosibirsk, 1986), 669, 65–76.
159. L. I. Egorova, Novye nizhnekembriyskie trilobity yugo-vostoka Sibirskoy platformy. *Paleontologicheskiy Zhurnal* **1983**, 59–64 (1983).
160. L. N. Repina, V. A. Luchinin, To the biostratigraphy of the lower part of the Lower Cambrian in northwestern Prinabar'e (R. Fomich) in *Boundary Strata of the Precambrian and Cambrian of the Siberian Platform (Biostratigraphy, Palaeontology, Conditions of the Formation*, N. P. Meshkova, I. V. Nikolaeva, eds. (Institut Geologii i Geofiziki Sibirskogo Otdeleniya Akademii Nauk SSSR, Trudy 475. Novosibirsk, Nauka, 1981) pp. 3–19 [in Russian].
161. L. Na, W. Kiessling, Diversity partitioning during the Cambrian radiation. *Proc. Natl. Acad. Sci. U.S.A.* **112**, 4702–4706 (2015).
162. M. dos Reis, Y. Thawornwattana, K. Angelis, M. J. Telford, P. C. J. Donoghue, Z. Yang, Uncertainty in the timing of origin of animals and the limits of precision in molecular timescales. *Curr. Biol.* **25**, 2939–2950 (2015).
163. T. H. Torsvik, L. R. M. Cocks, The integration of palaeomagnetism, the geological record and mantle tomography in the location of ancient continents. *Geol. Mag.* **156**, 242–260 (2019).
164. L. N. Repina, N. P. Lazarenko, N. P. Meshkova, V. I. Korshunov, N. I. Nikiforov, N. A. Aksarina, Biostratigraphy and Fauna of the Lower Cambrian of the Kharaulakh (Tuora-Sis Ridge). Trans. Inst. Geol. Geophys. Siberian Branch USSR Acad. Sci. 235 [in Russian] (Nauka, 1974).
165. V. A. Luchinina, I. V. Korovnikov, D. P. Sipin, A. V. Fedoseev, Biostratigraphy of the Upper Vendian-Lower Cambrian in the Sukharikha River section (Siberian Platform). *Geol. Geophys.* **38**, 1346–1358 (1997).
166. A. Kouchinsky, S. Bengtson, V. Pavlov, B. Runnegar, P. Torssander, E. Young, K. Ziegler, Carbon isotope stratigraphy of the Precambrian–Cambrian Sukharikha River section, northwestern Siberian platform. *Geol. Mag.* **144**, 609–618 (2007).
167. A. Kouchinsky, S. Bengtson, V. Pavlov, B. Runnegar, A. Val'kov, E. Young, Pre-Tommotian age of the lower Pestrotsvet Formation in the Selinde section on the Siberian platform: Carbon isotopic evidence. *Geol. Mag.* **142**, 319–325 (2005).

Acknowledgments: We thank U. Baranowski, S. Reid, Y. Xiong, F. Keay, and A. Hobson for technical support. **Funding:** This work was supported by NERC E4 DTP (R.D.A.), UKRI Projects NE/T008458/1 (R.W., S.W.P., and F.T.B.) and NE/Z000122/1 (R.W. and S.W.P.), and UKRI Project EP/Y008790/1 (F.T.B.). **Author contributions:** R.W., F.T.B., A.Y.Z., and R.D.A. conceived the project. A.K. collected samples. R.D.A. prepared samples for analysis. R.D.A., F.T.B., and L.P. conducted geochemical analyses. R.D.A., F.T.B., L.P., S.W.P., and R.W. interpreted the geochemical data. R.D.A. constructed the figures and wrote the first draft of the manuscript, and all authors contributed to the final paper. **Competing interests:** The authors declare that they have no competing interests. **Data and materials availability:** All data needed to evaluate the conclusions in the paper are present in the paper and/or the Supplementary Materials. For the purpose of open access, the authors have applied a Creative Commons Attribution (CC BY) licence to any author-accepted manuscript version arising.

Submitted 6 August 2024
Accepted 23 December 2024
Published 24 January 2025
10.1126/sciadv.ads2846